International Journal of Innovation Engineering and Science Research

Editorial Board

International Journal of Innovation Engineering and Science Research

Volume 4 ISSUE 4 July-August 2020

Evaluation of the Physico-Chemical Quality and Study of the Aggressivity of the Groundwater and Surface Water Exploited in Yaya District (NIARI Department, CONGO)

Essouli O. F. || Malanda Nimy E. N. || Miyouna T. || Moudzika Loubaki H. B. || Matini L. || Boudzoumou F. || Faye S.

Use of De-Aluminated Metakaolin Waste as A Supplementary Cementitious Material in Mortars

Dr. Enas A.A. Khattab

Implementation of statistical methods to the comparative study of heavy minerals of the Cover Formation and its bedrock in the Pointe-Noire and Brazzaville sectors (Republic of Congo)

Miyouna T. || Essouli. O. F. || Malanda Nimy E. N || Boudzoumou F. || Kendé M. || Mokono-Mboko C. || Sow E. H.

International Journal of Innovation Engineering and Science Research
(ISSN: 2581-4591)
www.ijiesr.com

Evaluation of the Physico-Chemical Quality and Study of the Aggressivity of the Groundwater and Surface Water Exploited in Yaya District (NIARI Department, CONGO)

Essouli O. F.[1,*], Malanda Nimy E. N.[1], Miyouna T.[1], Moudzika Loubaki H. B., Matini L.[2], Boudzoumou F.[1, 3], Faye S.[4]

[1]*Université Marien NGOUABI, Faculté des Sciences et Techniques, Laboratoire de Géosciences, B.P. 69 Brazzaville, Congo*
[2]*Université Marien NGOUABI, Ecole Nationale Supérieure, Laboratoire de Chimie, B.P. 69 Brazzaville, Congo*
[3]*Institut National de Recherches en Sciences Naturelles et Exactes, B.P. 2400 Brazzaville, Congo*
[4]*Université Cheikh Anta Diop, Faculté des Sciences et Techniques, Département de Géologie, B.P. 743 Dakar-Fan, Senegal*

ABSTRACT

The physico-chemical study of the groundwater and surface water of Yaya district revealed that these waters are fresh, weakly mineralized, under-saturated with respect to anhydrite, aragonite, calcite, dolomite and gypsum and the alkalinity of these waters is dominated by bicarbonate ions (HCO_3^-). These waters are also characterized by two (2) chemical families (calcium and magnesian chlorinated and sulphated waters and calcium and magnesian bicarbonate waters). From the chemical facies point of view, surface and ground waters are mainly characterised by chemical facies of the magnesian sulphate and chlorinated and calcium and magnesian sulphate type. In terms of quality, the good potability of water is called into question by the presence of certain elements such as total iron (Fe_{tot}), hexavalent chromium (Cr^{6+}), lead (Pb^{2+}) and aluminium (Al^{3+}) at levels that sometimes exceed the maximum permissible concentrations for drinking water defined by the WHO. Finally, the determination of the aggressive character of groundwater and surface water revealed that these waters are aggressive and very highly corrosive.

Keywords: Hydrochemistry, physico-chemistry, chemical facies, water quality, aggressiveness

I. INTRODUCTION

In Congo, the drinking water supply of several localities depends on groundwater. To improve the quality of life and hygiene of the population of the Yaya district in Niari department, several hydraulic boreholes have been drilled, some equipped with human-powered pumps (PMH) and others with photovoltaic pumps. The lack of information on the physico-chemical characteristics of the ground and surface waters of Yaya district constitutes a health hazard for the populations who get their water from boreholes and surface waters because these physico-chemical characteristics provide necessary information on water quality. However, the equipment of the various boreholes in this district is not always adapted to the physico-chemical characteristics of the groundwater and rocks crossed. Although the groundwater is still of acceptable chemical and bacteriological quality, it very often poses problems of aggressiveness. These problems and the solutions applicable to them are closely related to the chemical composition of the water and the nature of the geological formations crossed.

This study focuses on the evolution of the physico-chemical characteristics of the ground and surface waters of the Yaya district as well as on the determination of the aggressive character of these waters in relation to the different geological facies. The specific objectives are to determine the chemical quality and the Langelier and Ryznar indices of the ground and surface waters of the Yaya district for a better understanding of the phenomenon of aggressiveness and a precision in the choice of dewatering columns (steel casings and pumps) for the equipment of new future boreholes in this part of Congo.

II. MATERIAL AND METHODS OF THE STUDY

2.1. General Presentation of the Study Area

The district of Yaya is located in the south-west of Congo, more precisely in the department of Niari. It is bordered to the east and south-east by the Mpoukou River and to the south-west and west by the Louessé River. Specifically, the Yaya district lies between parallels 12°7' and 13°03' east longitudes and 3°00' and 3°03' south latitudes (**Figure 1**).

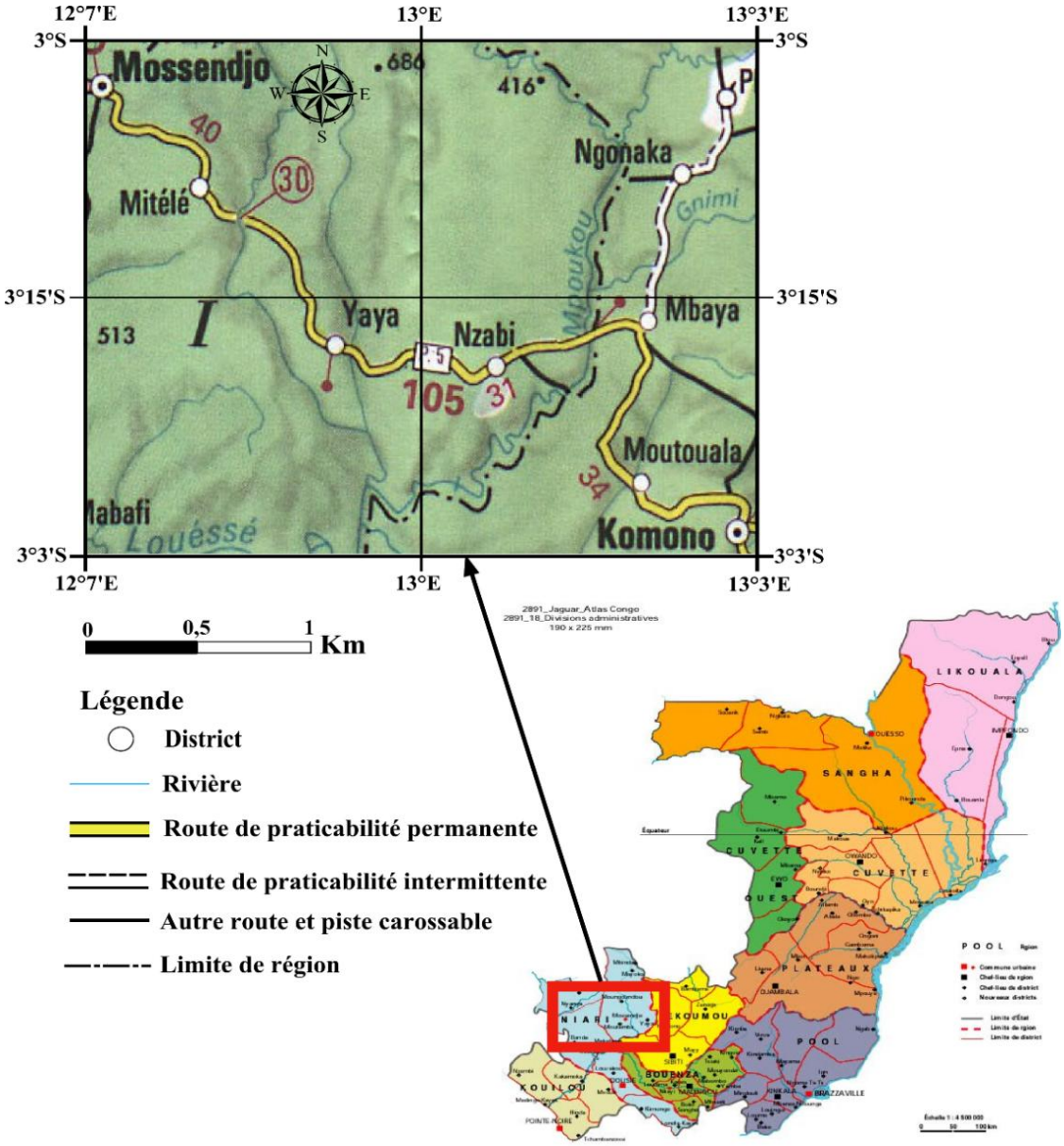

Figure 1. Location map of the study zone **[1]**

The Yaya district is characterized by a humid tropical climate due to its geographical position and relief. Annual rainfall varies between 1200 mm and 1800 mm and the interannual average from 2001 to 2013 is 1600 mm/year. These important precipitations can be explained by the fact that the atmospheric conditions are favourable (preponderance of low intertropical pressures, non-subsidized maritime trade winds and the intensity of thermal convection) and the relatively high relief **[2]**.

The district of Yaya is located in the Chaillu Massif, which is characterized by a plateau relief with a low relief and an average altitude of 500 m, reaching an altitude of 850 m in places. It is also marked by stepped levels of erosion under an almost continuous forest mantle, short hills and ranges framed by a very tight hydrographic network and narrow valleys with waterfalls and rapids indicating one or more rejuvenations. Collectors often have a rectilinear course over part of their course, following tectonic directions, mainly north-south, interrupted by bends **[3]**.

2.1.2. Geological Setting of Yaya District

Situated on the south-eastern edge of the Chaillu massif and close to the Bouenzien outcrop area, the Yaya district is essentially made up of the formations of the latter according to the geological map drawn up by **[4]** and **[3]**.

It is therefore important to carry out a litho-stratigraphic reconnaissance of the geological formations of the Chaillu massif and those of the Bouenzien as well as their tectonic structures in order to interpret the hydrogeological data in a way that is closer to the characteristics of our aquifer.

2.1.2.1. The Formations of the Chaillu Massif

The Chaillu Massif is located in the south-west of Congo, and covers an area of about 25,000 km2. It is defined as a granitoid complex of Meso to Neo-Archean age in which volcano-sedimentary rocks are individualized to form greenstone belts associated with gneisses and intrusive rocks.

The Chaillu Massif appears to be in a cartographic discordance with the Phanerozoic formations of the Batéké Plateaux to the east. On Gabonese territory, the Francevillian series are added to this boundary, which also constitute the northern limit of the basement **[6]**. To the west, it follows the cover formations of western Congo via the Bouenzian underlying this cover. It is a cartographic contact or discordance with these formations, of which the Niari basin of upper Proterozoic age is represented in Gabon by the Nyanga basin. This cover, together with the Bouenzien, also marks the southern limit of this massif **[6]**.

The granitisation of the Chaillu massif has spared some metamorphic sectors, appearing in kilometric massifs and hectometric to metric enclaves **[7]**. They are visible as an elongated structure, oriented northeast southwest in the west of the Chaillu (with a geometric appearance) and north-south in the east of the Chaillu, over a distance of about 30 km. The magmatic formations are represented by granitoid and peridotitic facies. Gneiss and migmatite accompany the magmatic rocks. It is associated with the previous group by amphibolites, pyroxenites, a schistose facies and ferruginous, banded and metamorphosed quartzites or BIF.

From a tectonic and structural point of view, the examination of aerial photographs revealed three (3) fracture directions **[8]**; **[3]**, namely:

- a frequent north-south meridian direction to the north and north-east of the massif. This fracture direction mainly concerns the small arteries, and is thought to be related to the effects of diaclases;

- a frequent NE-SW direction in the centre and west. This is the direction followed by most of the rivers such as the Nianga, the Louessé and the Mpoukou;

- a north-western direction which is mainly represented in the south of the Chaillu Massif.

2.1.2.2. The Geological Formations of the Bouenzien

The Bouenzien outcrops on the southeastern edge of the Chaillu Massif is part of the super group of western Congo where its lateral equivalent is the Louila formation **[9]**.

However, from a genetic point of view **[10]** attributes this geological formation to a detrital series containing subcontinental and sometimes coastal facies indicating sedimentation at the edge of a desert continent.

From a lithological point of view, the most complete succession of the Bouenzien has been described in the locality of Sibiti by **[11]** where it is constituted from bottom to top by: a schistose argillite (BZ1), a feldspathic sandstone (BZ2), a marly limestone (BZ3) and a calcareous sandstone (BZ4).

According to **[3]**, "the Bouenzien series lies in major discordance on the Chaillu granite complex". In the large morphological depressions in the valleys, a small metric level of fine arkosic sandstone, locally coarse, with conglomeratic lenses, is locally observed in contact with the granite, where the clays of the upper level lie directly on the substratum. Furthermore, on the southwestern flank of Chaillu the series is subhorizontal while on the southeastern flank it is folded. In addition to this, lateral variations in facies and truncations mean that the lithology of the Bouenzien varies according to the locality chosen. For our locality, we will refer to the lithology described by **[10]**. The latter noted the presence of only two (2) lower levels of the series, namely: the BZ1 which consists of reddish argillite with sandstone lenses and locally a thin sandstone bank (arkose) in contact with the granite and finally an upper level BZ2. It evokes the difficulty of tracing the contours of the Bouenzien in general and those of its four (4) levels in particular due to the aspects mentioned above, added to these the rarity of intact outcrops and the similarities of the facies of levels BZ1 and BZ3 on the one hand and BZ2 and BZ4 on the other.

From a regional geological standpoint, the upper tillite lies in continuity to the west and in gullying discontinuity to the east over the Bouenzien series, and this tillite supports the schistose limestone and Mpioka group **[3]**; **[12]**.

From a tectonic point of view, the Bouenzian, which belongs to the extreme foreland, shows almost no metamorphism except for a few fold schistosites.

2.1.3. Hydrogeological Context

In Congo, one distinguishes two (2) hydrogeological contexts: sedimentary regions with generalized aquifers formed essentially by loose sedimentary rocks, very little or not consolidated having a porosity of interstice i.e. with very appreciable hydrogeological potentialities and covering the 70 % of the territory and crystalline regions having a porosity of fissures, with random resources, whose aquifers are discontinuous and formed of compact and indurated sedimentary rocks, magmatic and metamorphic rocks and covering the 30 % of the territory.

The permanence of these aquifers depends on climatic regimes, modes of feeding, and the intrinsic hydrogeological and geological contexts of the environment. The Yaya district belongs to the latter context, i.e. crystalline regions, and the crystalline rocks that act as aquifers there are very diverse from the petrographic point of view. In spite of this great diversity, these rocks show a comparable hydrogeological behaviour because in a healthy state they have a great compactness which confers them a porosity and a permeability quasi zero. We see here, the primordial role of the network of local and regional fractures on the one hand, and on the other hand, that of the porosity and permeability of the altered fringe in the system of collection and accumulation of groundwater.

Thus, the work carried out by **[13]** on the "Hydrogeological characterization of exploited aquifers in Yaya district", revealed that it was a discontinuous aquifer. This result is also consistent with previous studies by **[14]** on the hydrogeological map of Africa and **[2]** on the hydrogeology of Congo.

The judicious analysis of the synthetic lithological sections of the various drill holes (**Figure 2**) shows the presence of a thick argilo-silt and lateritic cover that lies on a clay-lateritic to sandy level and the

latter, lies on a medium to coarse sandy level. The whole is supported by a substratum made up of blackish arkosic sandstone.

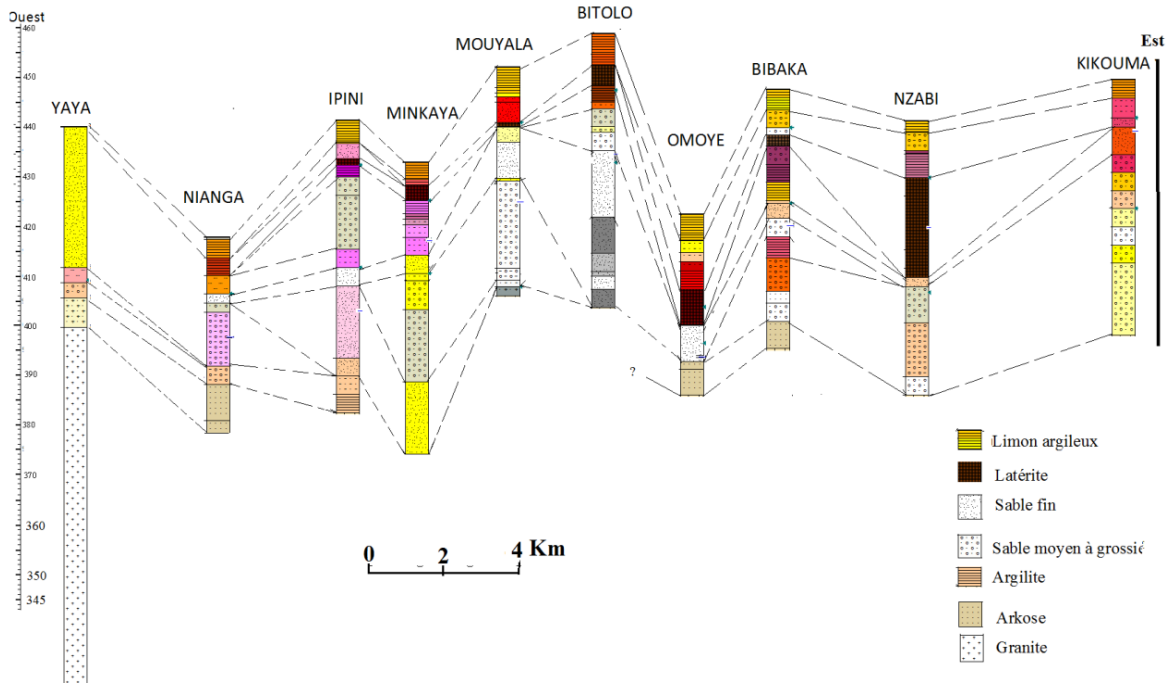

Figure 2. Lithological correlation of the different boreholes drilled in the Yaya district **[12]**

2.2. Methodology used

2.2.1. Acquisition of study data

For this study, samples were taken from more than thirty water points (boreholes, springs and rivers) in Yaya district in August 2015 (dry season) for the first season and in January 2017 (rainy season) for the second season (**Figures 3 and 4)**.

However, it is important to note that, depending on the different types of water, one sample was taken from each borehole and/or spring and two samples were taken from the watercourses (upstream or downstream) depending on whether the sampling was done at the level of the structures on the watercourses (bridges or dallos) or on the right and left banks when there were no geotechnical structures on the watercourses.

2.2.2. Laboratory phase

Samples taken in the field were then sent to the IRSEN laboratory for analysis. At the laboratory, pH and electrical conductivity were determined and the following elements were chemically analysed: Cl^-, SO_4^{2-}, NO_3^-, HCO_3^-, PO_4^{3-}, F^-, Na^+, K^+, Mg^{2+}, Ca^{2+}, Al^{3+}, Pb^{2+}, total iron (Fe_{tot}) and Cr^{6+}.

The pH and electrical conductivity were determined using a pH meter and a conductivity meter, respectively. The chemical analyses of Cl^-, SO_4^{2-}, NO_3^-, Na^+, K^+, Mg^{2+} and Ca^{2+} ions were carried out using a PC7000 type photometer; those of Al^{3+}, Pb^{2+}, F^-, PO_4^{3-}, total iron (Fe_{tot}) and Cr^{6+} ions were carried out using a Lovibond type spectrodirect and those of bicarbonate ions (HCO3-) by titrimetry.

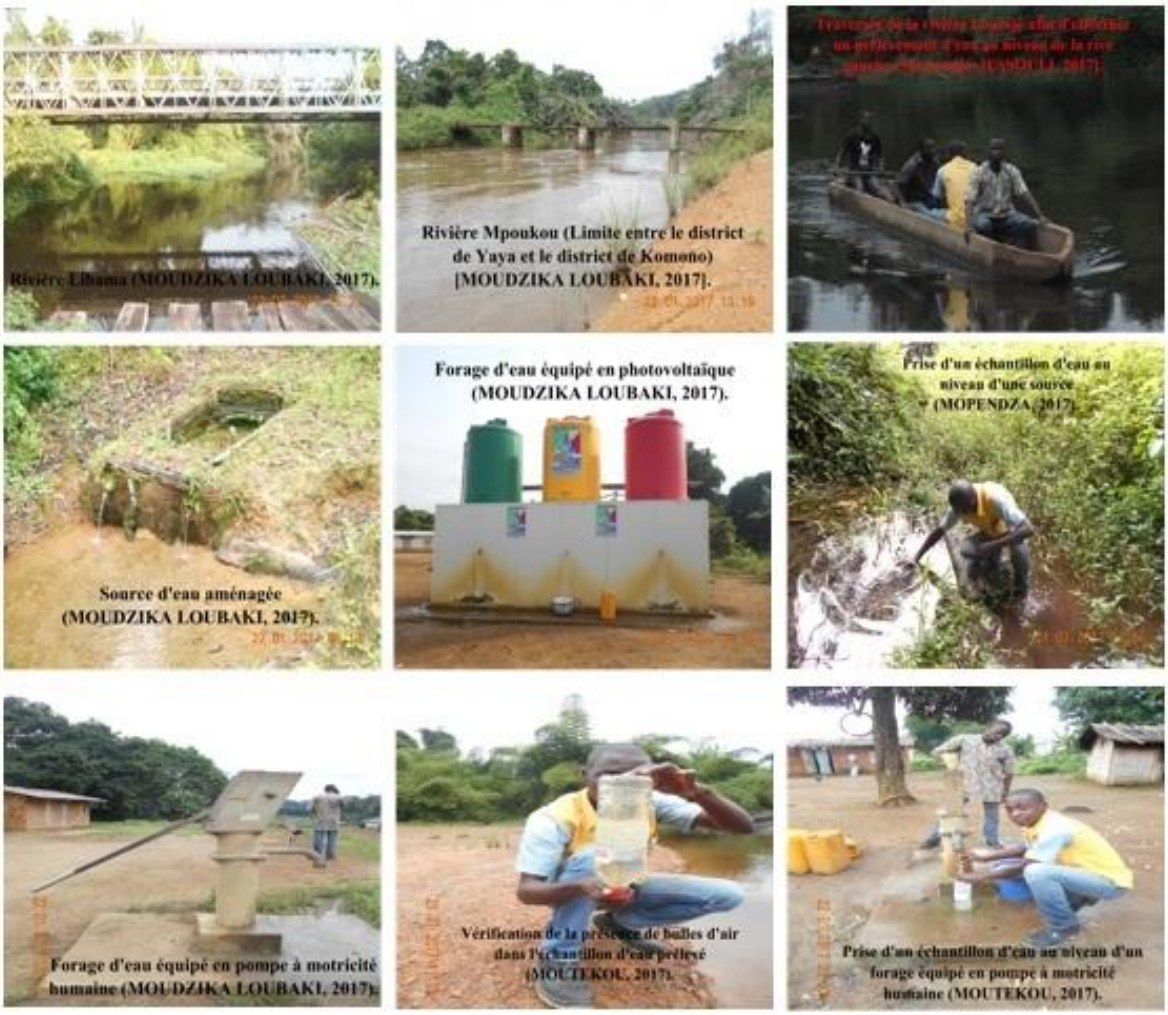

Figure 3. Different groundwater and surface water abstraction points in Yaya District [1]

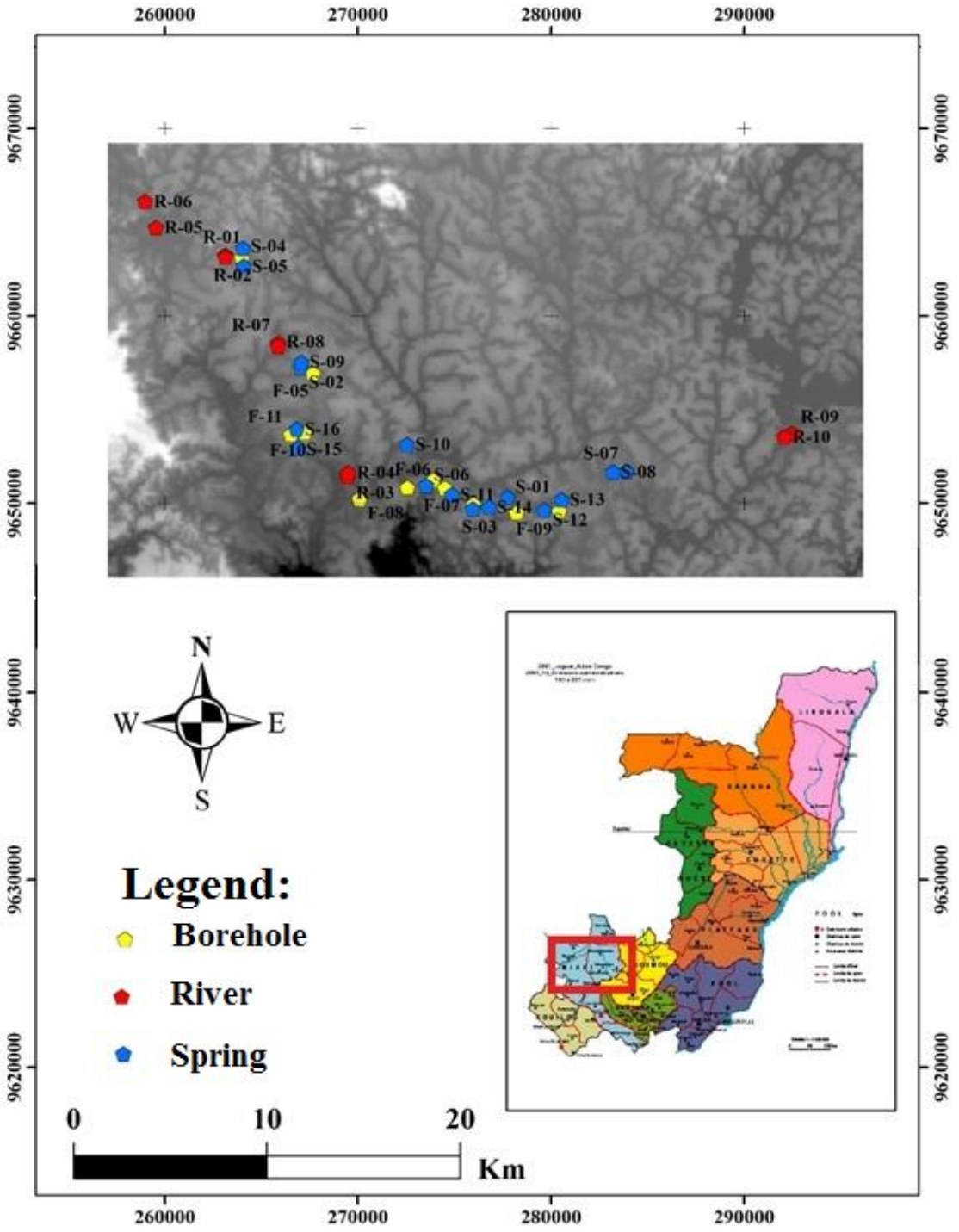

Figure 4. Location of groundwater and surface water sampling points in Yaya District [1]

2.2.3. Data processing

2.2.3.1. Verification of the ionic balance

The solutions are electrically balanced and therefore the sum of the positive charges is equal to the sum of the negative charges. The ionic balance must be correct, i.e. the sum of the cationic charges must be equal to the sum of the anionic charges.

Before any data processing, the calculation of the ionic balance, which is the relative difference between the sum of the cations and the sum of the anions, is indispensable because it allows the accuracy of the analytical methods used and the validity of the chemical determinations to be verified **[15]**; **[16]**. If the relative deviation is less than 5%, the analyses can be considered good. When the value is between 5% and 10%, the analyses may be retained. Above 10 %, the analyses should be rejected because there were errors in sampling or the analytical methods are imprecise or one or more elements in solution have not been determined.

In our study, the ion balances were less than 5% over all the analyses performed, which is a testimony to the good quality of the analyses. The collected data were then processed by different methods of interpretation of the hydrochemical data.

2.2.3.2. Study of the aggressiveness of groundwater and surface water in the Yaya district

The phenomenon of water aggressiveness has been studied by several authors who have proposed methods for its qualitative and quantitative evaluation. These authors include Langelier, Ryznar, Larson, Stiff and Davis for qualitative methods; Hallopeau-Dubin, Girard, for quantitative methods. However, in the case of this study, we have chosen the stability indices of Langelier and Ryznar.

Langelier Stability Index (LSI)

The Langelier Index is a measure of the involvement of the chemical quality of the water in the premature destruction of strainers, pumps and water pipes.

Langelier assesses the aggressiveness of the water using as data the total salinity or dry residue at 110°C, temperature, calcium content and alkalinity. He thus calculates the pH that the solution should have to be in equilibrium with the calcium carbonate. By comparing the calculated value with the pH of the water, he determines whether the water is aggressive or encrusting, thus defining an aggressiveness index:

$$ISL=pHmes-pHsat$$

With: pHmeas = pH measured in the field and pHsat = pH saturation (calculated) from the chart software.

Table 1 below shows the relationship between Langelier stability index values and the aggressive tendency of the water.

Langelier Stability Indexes	Aggressive Water Trend
$IS_L>0$	Scaling or encrusting waters. This phenomenon can lead to clogging of certain parts of the collecting system, which considerably reduces the pumping flow rate.
$IS_L=0$	Water in balance
$IS_L<0$	Aggressive waters and can attack metal equipment in water pipes.

Ryznar Stability Index

The Ryznar stability index is an empirical expression that determines the corrosive tendency of water and is calculated by the following formula:

$$SRI = S - C\text{-}pH = 2pHsat - pHmes$$

With:

SRI: Ryznar stability index; pHsat = pH saturation (calculated); pHmes: measured pH; S: constant derived from dissolved solids;
C: constant derived from alkalinity and calcium.

Table 2 below shows the relationship between the Ryznar stability index and the corrosive tendency of the water:

IS_R	Trend
4 à 5	Heavy scaling
5 à 6	Low scaling
6 à 7	Equilibre
7 à 7,5	Slight corrosivity
7,5 à 8,5	High corrosivity
>8,5	Very high corrosivity

III. RESULTS AND DISCUSSION

3.1. Physico-chemical characteristics of groundwater and surface water

The present study, which deals with the data of the January 2017 campaign (**Table 3**) and the August 2015 campaign (**Table 4**), is taken up here with a view to estimating the spatial and temporal evolution of the mineralization of ground and surface water in the Yaya district.

Groundwater and surface water have pH values that range from 5 to 6.32 for groundwater and 6.07 to 7.08 for surface water. These recorded pH values indicate that groundwater and surface water are acidic to slightly neutral and that alkalinity is mainly controlled by bicarbonate ions (HCO_3^-).

Depending on the electrical conductivity, these waters have electrical conductivity values between 20 and 48 µS/cm for ground water and between 27 and 50 µS/cm for surface water. On the whole, they are weakly mineralized because the electrical conductivity values are lower than 250 µS/cm **[17]**.

Figure 5 shows the groundwater and surface water classification for the January 2017 and August 2015 campaigns based on Piper's triangular diagram.

The lozenge diagram of the January 2017 campaign shows that the surface and groundwater of Yaya District are characterized by two (2) chemical families, namely:

- the chemical family of calcium and magnesium chloride sulphates, which represents 95%;
- and the chemical family of calcium and magnesium bicarbonates which represents 5%.

However, the lozenge diagram of the August 2015 campaign shows that groundwater and surface water are characterized by four (4) chemical families, namely:

- the chemical family of calcium and magnesium chloride sulphates, which represents 47%;
- the chemical family of calcium and magnesium bicarbonates which represents 39%;
- the chemical family of sodium and potassium chlorides or sodium sulphate which represents 11%;
- the chemical family of sodium and potassium bicarbonates, which represents 3%.

The triangular diagram of the anions of the January 2017 campaign, shows a predominance of water points with evolution towards the sulphated pole which represent 52%; water points with evolution towards the pole with mixed facies i.e. where no anion dominates the other which represent 43% and two (2) water points with evolution towards the bicarbonate pole which represent 5%.

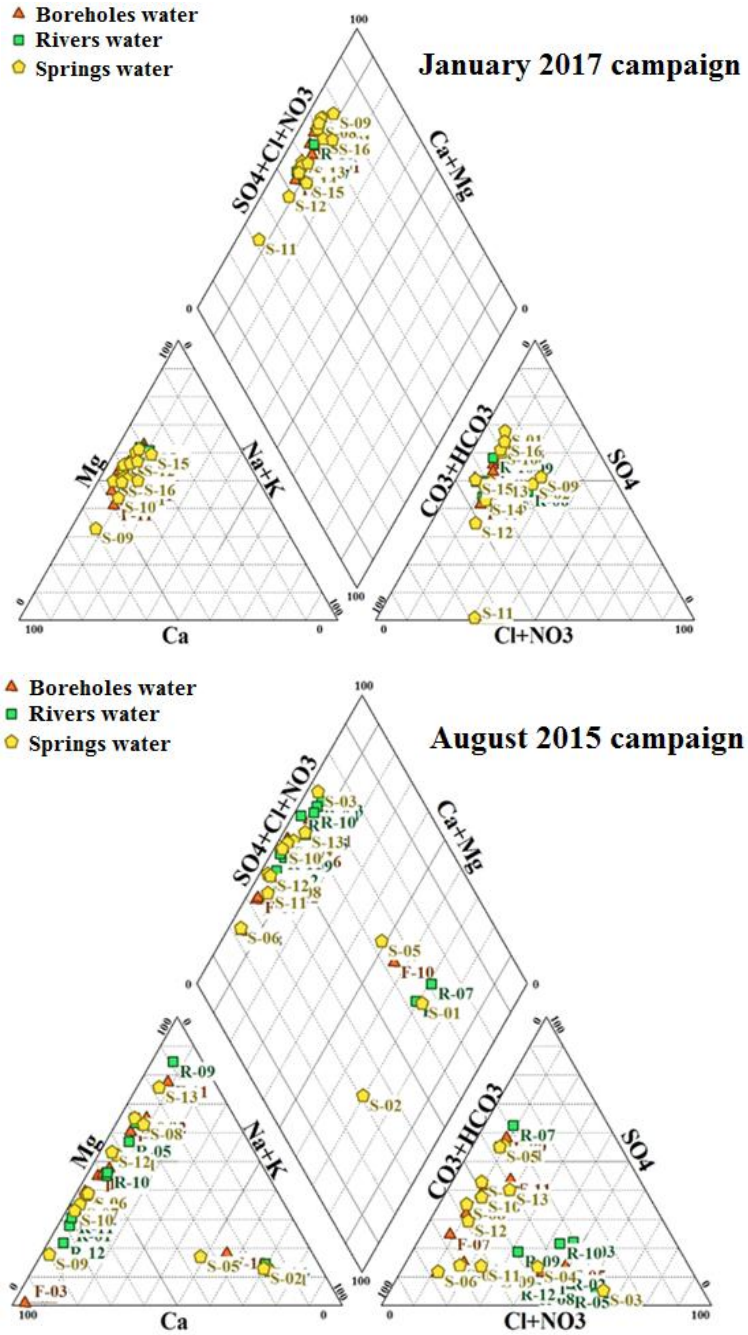

Figure 5. Classification of groundwater and surface water using Piper's triangular diagram **[1]**.

Contrary to the triangular diagram of the anions of the campaign of January 2017, that of August 2015, shows a predominance of the water points with evolution towards the bicarbonate pole which represent 42%; water points with evolution towards the pole with mixed facies i.e. where no anion dominates the other which represent 30%; water points with evolution towards the sulphated pole which represent 17% and four (4) water points with evolution towards the chlorinated pole which represent 11%.

Table 3. Results of physico-chemical analyses in mg/L of groundwater and surface water in Yaya district (January 2017)

Names of works	Labels	pH	EC (µS/cm)	TDS	Ca^{2+}	Mg^{2+}	Na^{+}	K^{+}	Cl^{-}	HCO_3^{-}	SO_4^{2-}	NO_3^{-}	Al^{3+}	Pb^{2+}	Fe_{tot}	Cr^{6+}	F^{-}	PO_4^{3-}
Bibaka village borehole	**F-01**	5,74	25	130	15	11	0,3	8,5	5,76	38,55	50,37	0,67	0,1	0,1	0,09	0,08	0,12	0,17
Bitolo village borehole	**F-02**	5,06	30	134	17	13	0,17	3,3	6,92	36,83	56,31	0,60	0,9	0,7	0,1	0,08	0,19	0,11
Gonaka village borehole	**F-03**	6,17	40	118	13	12	0,18	4	7,92	42,83	37,96	0,01	0,9	0,29	0,11	0,08	0,16	0,12
Ipini village borehole	**F-04**	6	20	121	17	10	0,15	3,9	5,18	37,83	46,51	0,73	0,1	0,8	0,7	0,07	0,18	0,13
Mikoubou village borehole	**F-05**	6,03	20	154	17	14	0,22	7	9,28	56,92	44,98	1,83	0,7	0,7	0,9	0,07	0,11	0,11
Mingaya village borehole	**F-06**	6,17	25	142	17	14	0,18	4	6,32	40,90	58,81	0,61	0,1	0,12	0,6	0,06	0,13	0,13
Mouyala village borehole	**F-07**	5,22	30	100	11	10	0,15	3,7	4,71	24,41	43,77	0,18	0,1	0,18	0,1	0,07	0,9	0,1
Nianga village borehole	**F-08**	5,6	30	116	10	13	0,14	5	7,10	47,37	33,28	0,24	0,7	0,3	0,09	0,06	0,16	0,15
Nzabi village borehole	**F-09**	6,02	24	109	13	10	0,18	5	5,62	35,20	40,28	0,10	0,13	0,11	0,1	0,08	0,12	0,17
Central Yaya borehole 1	**F-10**	6,07	30	115	10	12	0,13	6,5	3,29	42,98	39,88	0,12	0,9	0,2	0,8	0,08	0,16	0,22
Central Yaya borehole 2	**F-11**	5,82	25	138	20	10	0,18	6,9	6,76	39,79	53,95	0,48	0,1	0,1	0,08	0,09	0,9	0,15
Gonaka river (Upstream)	**R-01**	6,17	50	118	11	13	0,18	4,7	7,32	42,98	38,60	0,16	0,9	0,21	0,08	0,06	0,17	0,15
Gonaka river (Downstream)	**R-02**	6,25	45	108	10	12	0,17	4	6,33	42,36	33,25	0,05	0,6	0,19	0,06	0,07	0,15	0,11
Libama river (Upstream)	**R-03**	6,20	40	102	9	11	0,12	5,2	3,84	38,18	35,02	0,07	0,13	0,4	0,9	0,06	0,16	0,13
Libama river (Downstream)	**R-04**	6,22	30	110	10	12	0,1	4,9	6,95	42,06	33,54	0,14	0,1	0,32	0,8	0,07	0,17	0,18
Louesse river (left strand)	**R-05**	6,07	50	134	18	11	0,19	8	17,18	35,38	43,69	0,49	0,15	0,35	0,13	0,11	0,18	0,2
Louesse river (right strand)	**R-06**	7,02	50	154	19	11,8	0,19	8,4	18,17	37,47	46,74	0,54	0,16	0,35	0,13	0,11	0,18	0,22
Moutamba river (Upstream)	**R-07**	7,05	40	95	9	10	0,11	5	5,06	33,22	32,79	0,19	0,12	0,18	0,09	0,07	0,17	0,2
Moutamba river (Downstream)	**R-08**	6,42	50	86	7	9	0,13	4,8	2,77	31,71	28,20	0,07	0,1	0,25	0,08	0,06	0,13	0,14
Mpoukou river (left strand)	**R-09**	7,08	28	108	12	11	0,17	4,7	7,76	27,64	44,20	0,50	0,12	0,28	0,9	0,12	0,15	0,2
Mpoukou river (right strand)	**R-10**	7,06	27	123	15	11	0,1	5	3,00	36,63	49,00	3,18	0,9	0,17	0,7	0,06	0,13	0,26
Bibaka village spring	**S-01**	6,00	20	145	18	12	0,33	8,7	4,54	32,63	68,02	0,91	0,11	0,13	0,09	0,05	0,13	0,13
Bibayi village spring	**S-02**	5,32	25	136	17	14	0,18	4,1	18,08	33,58	48,76	0,35	0,1	0,12	0,8	0,09	0,19	0,18
Bitolo village spring	**S-03**	5,00	20	132	18	12	0,16	3,4	6,47	32,72	58,64	0,65	0,8	0,8	0,11	0,09	0,2	0,15
Gonaka village spring 1	**S-04**	6,00	30	111	11	12	0,18	3,9	6,85	40,74	36,26	0,13	0,1	0,3	0,1	0,09	0,14	0,13
Gonaka village spring 2	**S-05**	6,02	48	127	12	14	0,2	4,9	8,93	47,91	39,22	0,15	0,1	0,28	0,09	0,08	0,14	0,1
Ipini village spring	**S-06**	5,17	25	123	15	11	0,17	4,8	5,70	44,56	40,84	0,74	0,7	0,1	0,8	0,05	0,16	0,12

Kikouma village spring 1	**S-07**	6,13	39	138	16	14	0,2	4,2	6,68	37,73	58,79	0,50	0,12	0,1	0,12	0,07	0,2	0,42
Kikouma village spring 2	**S-08**	6,32	40	118	14	12	0,19	3,2	5,76	30,66	51,68	0,34	0,11	0,9	0,9	0,06	0,2	0,11
Mikoubou village spring	**S-09**	6,00	20	85	15	5	0,2	3,5	11,15	16,82	29,98	0,32	0,12	0,17	0,9	0,07	0,15	0,18
Mingaya village spring	**S-10**	6,13	30	116	16	9	0,2	5,8	4,92	30,70	48,78	0,39	0,9	0,12	0,7	0,05	0,14	0,14
Mouyala village spring	**S-11**	5,30	33	111	12	11	0,18	4	16,77	66,08	0,69	0,57	0,12	0,25	0,12	0,08	0,12	0,16
Nzabi village spring	**S-12**	5,77	35	110	11	11	0,15	5,2	7,71	48,90	26,10	0,01	0,1	0,27	0,06	0,07	0,1	0,1
Nzabi village spring	**S-13**	5,90	22	100	12	9	0,16	4,8	5,73	34,46	34,09	0,02	0,11	0,9	0,9	0,07	0,11	0,15
Omoye village spring	**S-14**	6,05	40	103	13	9	0,13	4,2	6,71	39,66	30,39	0,16	0,9	0,13	0,7	0,06	0,14	0,13
Central Yaya spring 1	**S-15**	6,01	28	96	8	10	0,11	6,2	3,03	35,87	32,72	0,02	0,7	0,17	0,7	0,09	0,14	0,18
Central Yaya spring	**S-16**	5,70	25	89	10	8	0,16	6	3,79	21,76	39,56	0,16	0,8	0,15	0,08	0,07	0,13	0,15

Table 4. Results of physico-chemical analyses in mg/L of ground and surface water in Yaya district (August 2015 campaign)

Names of works	Labels	pH	EC (µS/cm)	TDS	Ca^{2+}	Mg^{2+}	K^{+}	Na^{+}	HCO_3^{-}	Cl^{-}	SO_4^{2-}	NO_3^{-}	Fe_{tot}	Al^{3+}	PO_4^{3-}	Mn^{2+}	NH_4^{+}	Cu^{2+}
Bibaka village borehole	**F-01**	5	13	182	30	12,4	1,2	0,72	74,04	6,27	51,01	6,12	0,01	0,02	0,06	0,16	0,04	0,9
Bibayi village borehole	**F-02**	4,38	14	112	8,5	12,5	2,7	1,4	55,45	3,83	23,76	2,62	0,031	0,018	0,07	0,36	0,012	0,48
Bitolo village borehole	**F-03**	5	10	276	70	0,44	3	1,16	149,07	18,44	25,77	7,18	0,09	0,012	0,07	0,3	<0,02	1,25
Mouyala village borehole	**F-04**	5,6	15	197	35	11	3	0,15	83,20	5,63	50,21	8,58	0,012	0,021	0,08	0,17	<0,02	0,015
Ipini village borehole	**F-05**	4,51	13	132	12,4	13,3	2,2	1,1	40,89	7,15	11,74	41,68	0,017	0,014	0,08	0,6	0,014	0,57
Gonaka village borehole	**F-06**	4,45	22	158	12,3	15,9	3,6	2,1	57,72	2,95	11,39	50,51	0,035	0,03	0,08	0,5	0,014	0,6
Kikouma village borehole	**F-07**	5,07	15	127	18	9,5	2,12	0,18	69,62	3,47	20,27	3,10	0,014	0,017	0,08	0,14	0,017	0,014
Nzabi village borehole	**F-08**	6,1	17	133	18	10	2,1	0,65	83,51	4,71	9,73	4,22	0,029	0,015	0,05	0,14	0,03	0,12
Boudzouka village borehole	**F-09**	4,43	13	132	18	11	2,2	1,25	38,04	3,45	52,68	4,13	0,012	0,019	0,07	0,17	<0,02	0,12
Mingaya village borehole	**F-10**	5	10	14	0,8	0,34	3	0,22	3,95	0,19	4,67	0,58	0,02	0,037	0,05	0,12	0,06	0,8
Central Yaya borehole	**F-11**	4,7	12	79	3,22	10,7	1,1	1,55	26,44	0,10	23,31	11,85	0,03	0,018	0,06	0,37	0,015	0,58
Libama river (right strand)	**R-02**	6,70	17	268	48,8	15,3	0,8	1,67	89,94	33,35	19,30	58,13	0,012	0,017	0,05	0,48	0,04	0,53
Libama river (left strand)	**R-09**	6,40	19	104	2,7	15	1,6	1,2	43,39	2,47	12,81	24,08	0,019	0,015	0,06	0,38	0,011	0,53
Louesse river (right strand)	**R-03**	6	20	214	30,3	17	2,1	3,14	57,50	24,90	32,64	46,33	0,02	0,01	0,08	0,28	0,07	0,55
Gonaka river (right strand)	**R-04**	5,7	19	125	10,7	13,3	1,65	1,3	34,10	8,22	3,46	51,79	0,026	0,027	0,06	0,39	0,012	0,52
Gonaka river (left strand)	**R-05**	4,65	10	123	12,2	11,6	1,87	1,6	41,51	7,26	3,66	42,73	0,026	0,028	0,05	0,41	0,013	0,55
Mpoukou river (right strand)	**R-06**	6,27	23	15	0,67	0,36	2,12	2,05	3,95	0,19	4,67	0,58	0,017	0,018	0,06	0,09	0,07	0,16
Mpoukou river (left strand)	**R-07**	6,1	24	16	0,7	0,33	3	1,75	3,25	0,17	5,51	0,70	0,018	0,017	0,07	0,2	0,07	0,14

Libama river (Ipini) (right strand)	**R-08**	6,94	13	130	10,8	14	1,8	0,85	54,92	5,71	4,68	36,44	0,009	0,016	0,06	0,45	0,012	0,55
Libama river (Ipini) (left strand)	**R-01**	6,14	17	332	60,2	14,8	1,6	2,7	124,07	15,37	13,10	100,13	0,012	0,018	0,09	0,34	0,05	0,48
Louesse river (left strand)	**R-10**	6,14	20	208	28,9	16,8	2,07	2,8	63,45	22,91	30,71	39,94	0,024	0,01	0,07	0,3	0,07	0,5
Moutamba river (right strand)	**R-11**	4,35	12	263	47	13	2,2	0,95	110,91	14,10	15,60	58,53	0,027	0,028	0,07	0,16	0,05	0,36
Moutamba river (left strand)	**R-12**	5,6	10	202	39	7	2,9	1,08	89,49	8,42	9,12	44,40	0,027	0,03	0,06	0,18	0,04	0,37
Mingaya village spring 2	**S-01**	4,9	13	16	0,72	0,33	1,8	2,6	4,12	0,23	5,11	0,75	0,018	0,013	0,08	0,1	0,06	0,1
Yaya central spring 2	**S-02**	4,74	15	21	0,98	0,44	2,25	3,18	10,14	0,80	1,61	1,12	0,013	0,015	0,08	0,11	0,04	0,13
Gonaka village spring	**S-03**	4,38	21	198	30	12	1,7	1	46,70	4,66	6,53	93,71	0,03	0,045	0,08	0,58	0,03	0,62
Ipini village spring	**S-04**	4,75	14	158	13,4	17,4	2	1,16	60,99	8,72	14,15	39,49	0,018	0,013	0,09	0,67	0,01	0,62
Kikouma village spring	**S-05**	5,7	12	14	1	0,3	2,25	0,3	3,95	0,19	4,67	0,58	0,027	0,048	0,08	0,18	0,05	0,11
Nzabi village spring	**S-06**	5,14	16	141	22	9	1,5	0,7	88,19	5,16	10,55	4,02	0,015	0,02	0,07	0,12	0,03	0,13
Bibaka village spring	**S-07**	4,75	15	167	29	10	1,14	0,96	68,02	4,23	47,62	5,29	0,013	0,026	0,05	0,14	0,03	0,1
Bibayi village spring	**S-08**	4,35	12	124	10	13,3	3	1,6	59,07	3,18	28,92	3,25	0,04	0,02	0,08	0,33	0,013	0,55
Bitolo village spring	**S-09**	4,4	12	370	82	11	2,7	1,45	184,43	44,06	28,46	14,43	0,01	0,019	0,06	0,14	<0,02	0,75
Mingaya village spring 1	**S-10**	4,25	10	236	42	13	2,9	0,18	99,74	6,20	58,15	12,45	0,08	0,04	0,05	0,13	0,03	0,6
Mouyala village spring	**S-11**	4,51	11	169	20	15	4	0,82	89,70	14,98	15,53	7,76	0,014	0,017	0,08	0,28	<0,02	0,28
Omoye village spring	**S-12**	6,12	13	123	15	11,2	2,17	0,16	61,34	4,40	24,00	4,57	0,01	0,03	0,07	0,2	0,03	0,017
Central Yaya spring 1	**S-13**	5,4	10	94	4,75	12,4	1,85	0,97	33,09	0,02	25,41	15,32	0,028	0,02	0,05	0,4	0,017	0,6

The triangular diagram of cations for the January 2017 campaign shows a predominance of water points with evolution towards the magnetic pole, which represent 70%; water points with evolution towards the pole with mixed facies, i.e., where no cation dominates the other, which represent 27%, and one water point with evolution towards the calcium pole (S-09, which represents 3%). In contrast to the triangular cation diagram of the January 2017 campaign, the August 2015 campaign shows a predominance of water points with evolution towards the calcium pole, which represent 36%; water points with evolution towards the magnetic pole, which also represent 36%; water points with evolution towards the pole with mixed facies, i.e. where no cation dominates the other, which represent 14% and water points with evolution towards the sodium and potassium pole, which also represent 14%.

The diagram (**Figure 6**) below shows the classification of ground and surface water in Yaya District for the campaigns of August 2015 and January 2017:

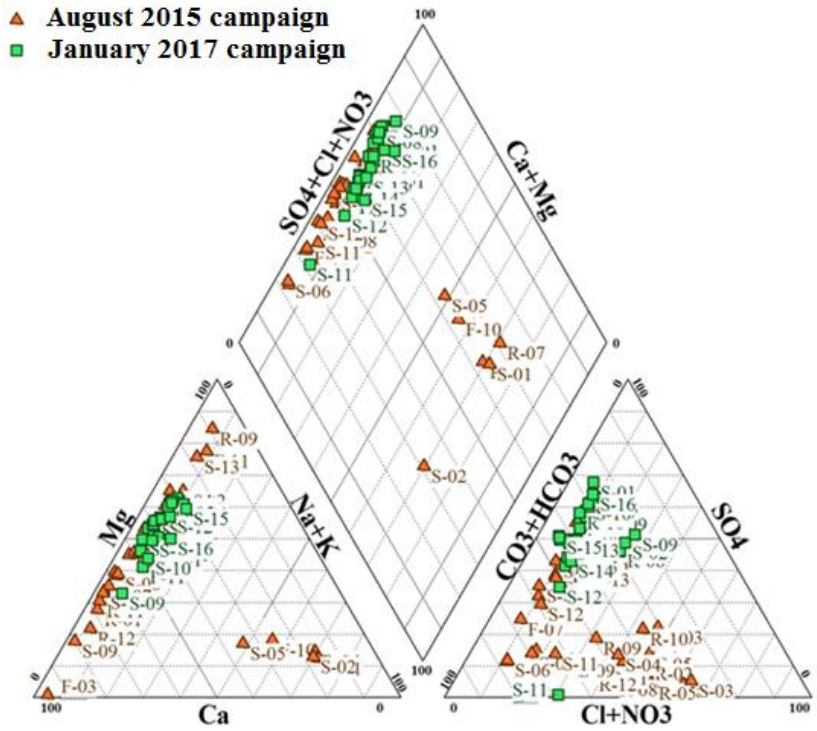

Figure 7. Evolution of water chemistry between August 2015 and January 2017 **[1]**

3.2. Ground and Surface Water Quality in Yaya District

Tables 5and 6 present the drinking water standards for some physico-chemical water parameters established by the World Health Organization **[18]** and the physico-chemical contents (minimum and maximum) of ground and surface water in Yaya District.

Figures 8 to **10** below show the variations in nitrate, magnesium, aluminium, lead, total iron and hexavalent chromium levels in the ground and surface waters of Yaya District.

Fluorine concentrations range from 0.1 to 0.9 mg/L for the January 2017 campaign and from 0.13 to 0.18 mg/L for the January 2017 campaign. As the WHO maximum allowable concentration value for fluoride in drinking water is 1.5 mg/L, all water points tested during both campaigns have fluoride levels that are below the WHO maximum allowable concentration for drinking water. However, fluoride concentrations below 0.5 mg/L in drinking water can promote dental caries **[19]**. However, at very high concentrations (above 1.5-2 mg/L), fluoride in drinking water can cause dental and/or bone fluorosis (**[20]**; **[21]**).

Total iron (FeTot) concentrations range from 0.06 to 0.9 mg/L for the January 2017 campaign and 0.06 to 0.12 mg/L for the August 2015 campaign. Since the WHO maximum allowable concentration value for total iron in drinking water is 0.3 mg/L, only 16 of the 37 water points tested in the January

2017 campaign have FeTot concentrations that exceed the WHO guideline value (**Figures 8c** and **9c**). Although iron is essential for the human body, very high iron concentrations affect the organoleptic properties of water and also stain laundry. In groundwater, iron can exist as soluble ferrous iron (Fe2+) or as insoluble ferric iron (Fe3+) which can be complexed, colloidal or precipitated. The presence of iron in water can promote the growth of certain strains of bacteria that precipitate iron or corrode pipes **[22]**.

Hexavalent chromium (Cr6+) concentrations range from 0.05 to 0.12 mg/L for the January 2017 campaign and from 0.06 to 0.12 mg/L for the August 2015 campaign. For both sampling campaigns, the chromium levels in the various water points analysed are greater than or equal to the maximum allowable concentration of 0.05 mg/L defined for drinking water by the WHO (**Figures 8** and **9**). Concentrations above this guideline value in drinking water can lead to skin rashes, gastric ulcers, a weakened immune system, and even lung cancer as a cumulative effect.

Lead (Pb^{2+}) levels range from 0.1 to 0.9 mg/L for the January 2017 campaign and 0.17 to 0.40 mg/L for the August 2015 campaign. Lead concentrations above the WHO drinking water potability guideline value can lead to brain and reproductive disorders, and the most severe type of lead poisoning leads to encephalopathy **[23]**.

Aluminum (Al^{3+}) concentrations range from 0.1 to 0.9 mg/L for the January 2017 campaign and 0.1 to 0.9 mg/L for the August 2015 campaign. Since the WHO drinking water guideline value for aluminum in drinking water is 0.1 mg/L, all water points tested have aluminum levels greater than or equal to the WHO drinking water guideline value (**Figures 9** and **10**).

Table 5.WHO (2004) potability standards and levels of physico-chemical groundwater parameters (January 2017 campaign)

Physico-chemical parameters	WHO (2004) maximum allowable values	Content of physico-chemical groundwater parameters	
		Minimum	Maximum
EC (µS/cm)	2000	20	48
pH	9,60	5	6,32
TDS (mg/L)	500	86	155
Ca^{2+} (mg/L)	100	8	20
Mg^{2+} (mg/L)	50	5	14
Na^{+} (mg/L)	100	0,11	0,33
K^{+} (mg/L)	12	3,20	8,70
Cl^{-} (mg/L)	200	3,03	18,08
HCO_3^{-} (mg/L)	-	16,82	66,08
NO_3^{-} (mg/L)	50	0,01	1,83
SO_4^{2-} (mg/L)	250	0,69	68,02
F^{-} (mg/L)	1,5	0,10	0,90
Fe_{tot} (mg/L)	0,3	0,06	0,9
Cr^{6+} (mg/L)	0,05	0,05	0,09
Pb^{2+} (mg/L)	0,01	0,10	0,9
Al^{3+} (mg/L)	0,1	0,10	0,9
PO_4^{3-} (mg/L)	0,5	0,10	0,42

Table 6. WHO (2004) potability standards and levels of physico-chemical parameters in surface waters (January 2017 campaign)

Physico-chemical parameters	WHO (2004) maximum allowable values	Contents of the physico-chemical parameters of surface waters	
		Minimum	Maximum
EC (µS/cm)	2000	27	50
pH	9,60	6,07	7,08
TDS (mg/L)	500	87	157
Ca^{2+} (mg/L)	100	7	19
Mg^{2+} (mg/L)	50	9	13
Na^{+} (mg/L)	100	0,10	0,19
K^{+} (mg/L)	12	4	8,40
Cl^{-} (mg/L)	200	2,77	18,17
HCO_3^{-} (mg/L)	-	27,64	42,98
NO_3^{-} (mg/L)	50	0,05	3,18
SO_4^{2-} (mg/L)	250	28,20	49
F^{-} (mg/L)	1,50	0,13	0,18
Fe_{tot} (mg/L)	0,30	0,06	0,90
Cr^{6+} (mg/L)	0,05	0,06	0,12
Pb^{2+} (mg/L)	0,01	0,17	0,40
Al^{3+} (mg/L)	0,10	0,10	0,90
PO_4^{3-} (mg/L)	0,50	0,11	0,26

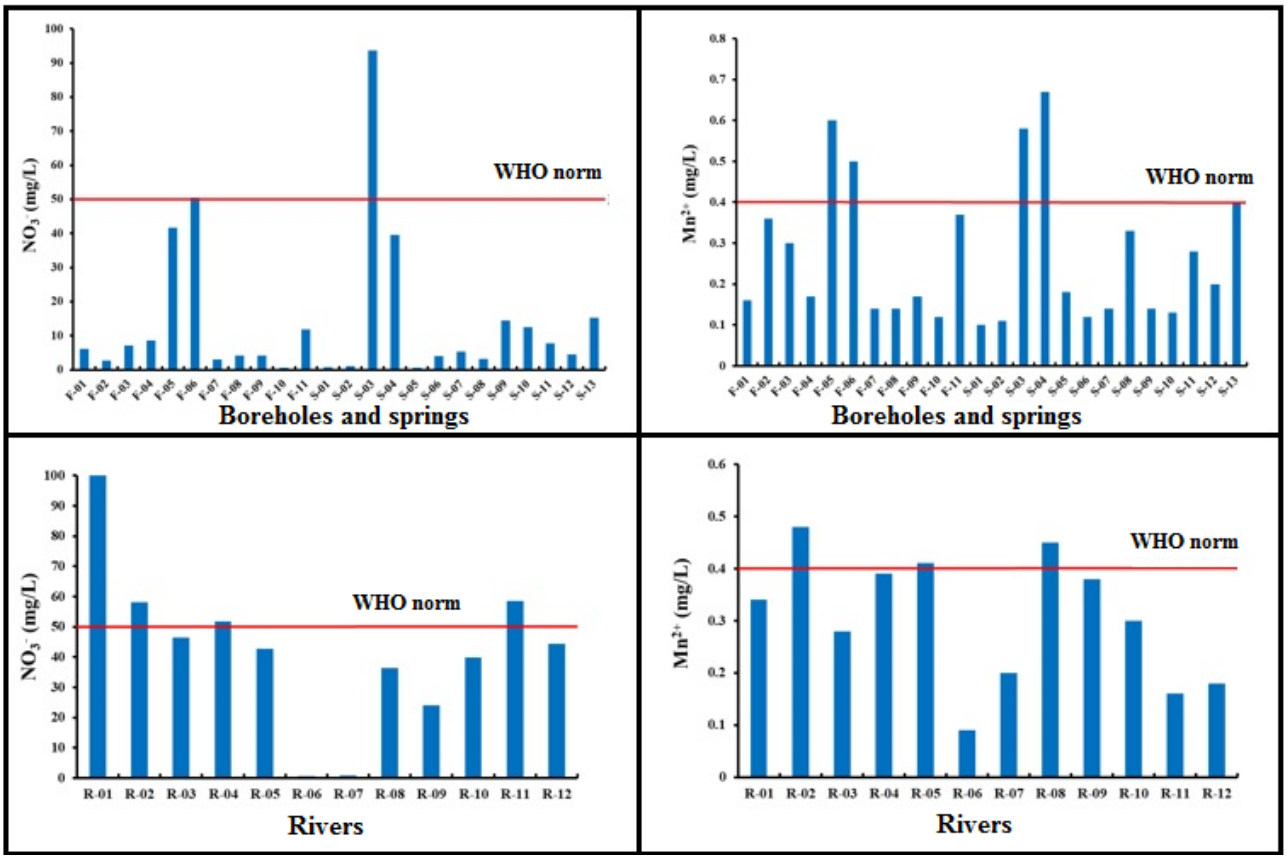

Figure 8. Variation of nitrate and manganese contents in groundwater and surface water for the August 2015 campaign **[1]**

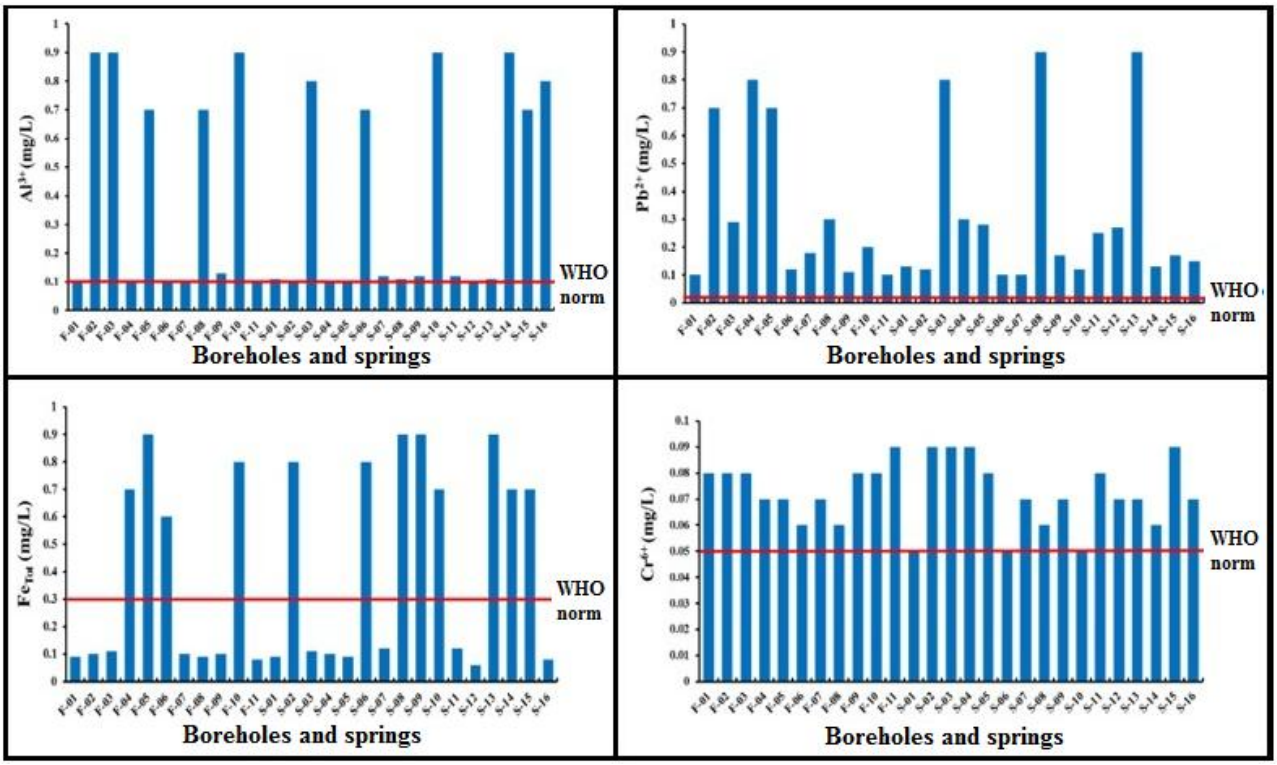

Figure 9. Diagrams of changes in the levels of aluminium, lead, total iron and chromium in groundwater [1]

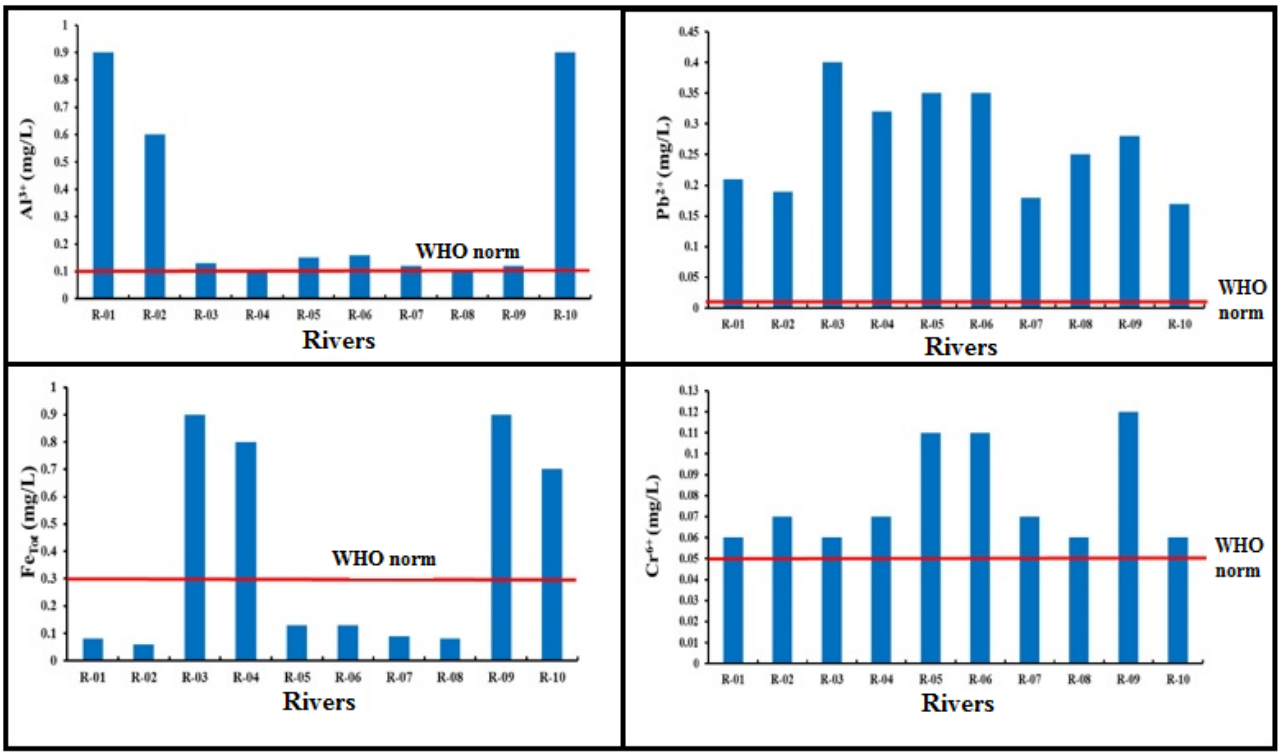

Figure 10. Diagrams of variation in the contents of aluminium, lead, total iron and chromium in surface waters [1]

3.3. Groundwater and surface water stress in Yaya District

Within the framework of this study, the Ryznar and Langelier indices for determining the aggressive character of the ground and surface waters of the Yaya district were determined using the

hydrogeochemical diagram software of Roland Simler from the University of Avignon. **Tables 7 and 8** below show the different values of the Ryznar and Langelier stability indices.

Table 7. Ryznar and Langelier stability index of groundwater and surface water (January 2017)

Names of works	Labels	IS_R (Ryznar)	IS_L (Langelier)
Bibaka village borehole	**F-01**	11,46	-2,86
Bitolo village borehole	**F-02**	12,09	-3,51
Gonaka village borehole	**F-03**	11,06	2,44
Ipini village borehole	**F-04**	11,11	-2,55
Kikouma village borehole	**F-05**	10,74	-2,36
Mingaya village borehole	**F-06**	10,89	-2,36
Mouyala village borehole	**F-07**	12,63	-3,70
Nianga village borehole	**F-08**	11,76	-3,08
Nzabi village borehole	**F-09**	11,37	-2,67
Yaya centre borehole 1	**F-10**	11,38	-2,65
Yaya centre borehole 2	**F-11**	11,12	-2,65
Gonaka river (Upstream)	**R-01**	11,20	-2,51
Gonaka river (Downstream)	**R-02**	11,20	-2,48
Libama river (Upstream)	**R-03**	11,43	-2,62
Libama river (Downstream)	**R-04**	11,24	-2,51
La Louessé river (left strand)	**R-05**	11,06	-2,49
La Louessé river (right strand)	**R-06**	10,03	-1,50
Moutamba river (Upstream)	**R-07**	10,69	-1,82
Moutamba river (Downstream)	**R-08**	11,57	-2,57
Mpoukou river (left strand)	**R-09**	10,59	-1,76
Mpoukou river (right strand)	**R-10**	10,18	-1,56
Bibaka village spring	**S-01**	11,21	-2,60
Bibayi village spring	**S-02**	11,91	-3,29
Bitolo village spring	**S-03**	12,20	-3,60
Gonaka village spring 1	**S-04**	11,41	-2,70
Gonaka village spring 2	**S-05**	11,19	-2,58
Ipini village spring	**S-06**	11,90	-3,37
Kikouma village spring 1	**S-07**	11,05	-2,46
Kikouma village spring 2	**S-08**	11,14	-2,41
Mikoubou village spring	**S-09**	11,88	-2,94
Mingaya village spring	**S-10**	11,21	-2,54
Mouyala village spring	**S-11**	11,60	-3,15
Nzabi village spring 1	**S-12**	11,47	-2,85
Nzabi village spring 2	**S-13**	11,57	-2,83
Omoye village spring	**S-14**	11,23	-2,59
Yaya centre spring 1	**S-15**	11,77	-2,88
Yaya centre spring 2	**S-16**	12,32	-3,31

Table 8. Ryznar and Langelier stability index of groundwater and surface water (August 2015).

Names of works	Labels	SRI (Ryznar)	SLI (Langelier)
Bibaka village borehole	**F-01**	12,69	-3,85
Bibayi village borehole	**F-02**	13,93	-4,74
Bitolo village borehole	**F-03**	11,51	-3,26
Mouyala village borehole	**F-04**	11,59	-2,66
Ipini village borehole	**F-05**	13,77	-4,66
Gonaka villageborehole	**F-06**	13,65	-4,60
Kikouma villageborehole	**F-07**	12,55	-3,74
Nzabi village borehole	**F-08**	11,52	-2,71
Boudzouka villageborehole	**F-09**	13,96	-4,77
Mingaya village borehole	**F-10**	15,90	-5,45
Central Yaya borehole	**F-11**	14,72	--5,01
Libama river (Ipini) (Upstream)	**R-01**	11,16	-2,11
Libama river (Ipini) (Downstream)	**R-02**	10,75	-2,31
Louesse river (left strand)	**R-03**	11,29	-2,65
Louesse river (right strand)	**R-04**	11,10	-2,48
Gonaka river (Upstream)	**R-05**	12,63	-3,47
Gonaka river (Downstream)	**R-06**	13,46	-4,41
Mpoukou river (right strand)	**R-07**	14,34	-4,04
Mpoukou river (left strand)	**R-08**	14,66	-4,28
Libama river bridge (Upstream)	**R-09**	10,33	-1,82
Libama river bridge (Downstream)	**R-10**	12,87	-2,94
Moutamba river (Upstream)	**R-11**	12,89	-4,27
Moutamba river (Downstream)	**R-12**	11,53	-2,97
Bibaka village spring	**S-01**	12,85	-4,05
Bibayi village spring	**S-02**	13,79	-4,72
Bitolo village spring	**S-03**	12,04	-3,82
Gonaka village spring	**S-04**	13,27	-4,45
Ipini village spring	**S-05**	13,04	-4,15
Kikouma village spring 1	**S-06**	14,85	-4,58
Mingaya village spring 1	**S-07**	12,94	-4,35
Mingaya village spring 2	**S-08**	15,53	-5,32
Mouyala village spring	**S-09**	13,27	-4,38
Nzabi village spring 1	**S-10**	12,33	-3,60
Omoye village spring	**S-11**	11,83	-2,86
Yaya central spring 1	**S-12**	13,44	-4,02
Yaya central spring 2	**S-13**	15,56	-5,41

3.3.1 Ryznar stability index (RSI)

The values of the Ryznar stability index of groundwater and surface waters of Yaya District for the January 2017 and August 2015 campaigns are on the whole higher than 8.5 (Tables 7 and 8). This means that the groundwater and surface water of Yaya District are very highly corrosive.

3.3.2 Langelier Stability Index

The values of Langelier stability index of groundwater and surface water in Yaya District for the January 2017 and August 2015 campaigns are on the whole below 0, which means that groundwater and surface water are aggressive, i.e. they dissolve calcium carbonate and can attack metal equipment in boreholes and water pipes.

3.4. Discussion

3.4.1. From the Physico-chemical Point of View

The study of physico-chemical parameters from the January 2017 sampling campaign of ground and surface waters of Yaya district located in Niari department, showed that these waters have pH values ranging between 5 (Bitolo village Spring) and 6.32 (Kikouma village Spring 2) for ground waters and between 6.07 (Louesse river) and 7.08 (Mpoukou river) for surface water. These recorded pH values indicate that the groundwater and surface waters of Yaya district are acidic to slightly neutral and that the alkalinity of these waters would be essentially controlled by bicarbonate ions (HCO_3^-). This result is in agreement with that of the August 2015 campaign, since their pH values ranged between 4.25 and 6.12 for groundwater and between 4.35 and 6.94 for surface waters **[24]**.

The total mineralization of groundwater and surface water as assessed by dissolved solids content (DST) measurements has shown that these waters are generally fresh, with DSTs ranging from 85 to 154 mg/L for groundwater and 86 to 154 mg/L for surface water. While based on electrical conductivity measurements, these waters are weakly mineralized as their electrical conductivities range from 20 to 48 50µS/cm for groundwater and 27 to 50 µS/cm for surface water. These results agree with those of the campaign of August 2015 where the groundwater and surface waters had TDS values between 14 and 370 mg/L for groundwater and between 15 and 332 mg/L for surface waters and electrical conductivity values between 10 and 22 µS/cm (Gonaka village borehole) for groundwater and from 10 µS/cm (Gonaka and Moutamba rivers) to 24 µS/cm (Mpoukou river) for surface water **[25]**.

From the point of view of chemical families and facies, the groundwater and surface water of the January 2017 campaign are characterized by two (2) chemical families (chlorinated and sulphated calcium and magnesian waters and bicarbonate calcium and magnesian waters) and are mainly represented by chemical facies of the sulphated magnesian and chlorinated and sulphated calcium and magnesian type. These results differ from those obtained by Poho Ngala during the August 2015 campaign where the ground and surface waters were characterized by four (4) chemical families (calcium and magnesian chlorinated-sulphated waters, calcium and magnesian bicarbonate waters, sodium and potassium chlorinated-sulphated waters and sodium and potassium bicarbonate waters) and were mainly represented by calcium and magnesian bicarbonate chemical facies.

Piper's triangular diagram of the evolution of water chemistry between the two sampling campaigns of August 2015 and January 2017 shows that there has been a change in the classification of water chemistry facies (**Figure 7**). The water points that were divided into four (4) chemical families (chlorinated-sulphate calcium and magnesian waters; bicarbonate calcium and magnesian waters; sodium and potassium chlorinated-sulphate waters and sodium and potassium bicarbonate waters) during the August 2015 campaign, and they are divided into two (2) chemical families (calcium and magnesium chlorinated-sulphate waters and calcium and magnesium bicarbonate waters) during the January 2017 campaign. This change in facies observed during the January 2017 campaign may be the result of an enrichment in chlorides, sulphates, calcium and magnesium (Mingaya borehole, Mpoukou river, Mingaya spring and spring 2 central Yaya) and a depletion in bicarbonates (boreholes in the villages of Bibayi, Bitolo, Kikouma, Mouyala and Nzabi ; Libama and Moutamba rivers; springs in the villages of Bibayi, Bitolo, Mouyala, Omoye, spring 1 in the village of Mingaya and spring 2 in the central Yaya), sodium and potassium (boreholes in the village of Mingaya, Mpoukou river and spring in the village of Mingaya).

The evolution of the sodium and potassium bicarbonate and sodium and potassium chloride sulphate chemical families towards the calcium and magnesium chloride and sulphate chemical family would probably be due to an enrichment in chlorides, sulphates, calcium and magnesium and a depletion in bicarbonates, sodium and potassium of the ground and surface waters between the two (2) campaigns. Chloride and sulphate enrichment would likely be the result of rock weathering or dissolution during the rainy season (high-water period) of the rock minerals in the area or through soil leaching.

3.4.2. From the Point of View of Chemical Quality

The comparative analysis of the physico-chemical parameters of the ground and surface waters of Yaya District with the values of maximum acceptable concentrations defined for drinking water by the WHO (**Tables 2** and **3)**, makes it possible to say that the good potability of these waters, is called into question by the presence of certain elements such as total iron (Fe_{tot}), hexavalent chromium (Cr^{6+}), aluminium (Al^{3+}) and lead (Pb^{2+}), the levels of which sometimes exceed the maximum admissible concentrations defined for drinking water by the WHO.

In addition, one of the most important health-related elements in drinking water is fluoride. Fluoride is present in water in the form of fluoride ions (F^-). Fluoride in water comes mainly from the dissolution of natural minerals present in rocks and soils with which water reacts **[26]**. Fluorite (CaF_2), cryolite (Na_3AlF_6), fluo apatite [$Ca_5F(PO_4)$] and micas are the main minerals that contain fluorine.

3.4.3. From the Point of View of Water Aggressiveness

Aggression is a complex phenomenon involving several factors of a chemical, electrochemical and even microbiological nature. The multiplicity of these factors makes the study of these problems extremely complex.

Indeed, the determination of the aggressive character of the ground and surface waters of Yaya district from the Langelier and Ryznar indices, allowed us to know that the ground and surface waters of Yaya district are aggressive and very strongly corrosive, i.e. they dissolve calcium carbonate and can attack the metallic equipment of the boreholes. On this basis, we recommend to the drilling companies the use of PVC pipes for the piping of the water distribution network for the entire service system.

IV. CONCLUSION

The study of the physico-chemical parameters of ground and surface water in Yaya district located in Niari Department revealed the following information:

- Ground and surface waters of the Yaya district are mild, weakly mineralized with acidic to slightly neutral pH values and the alkalinity of these waters is dominated by bicarbonate ions (HCO3-). Ground and surface waters of Yaya District are undersaturated with respect to anhydrite, aragonite, calcite, dolomite and gypsum;

- The ground and surface waters of Yaya district are characterized by two (2) chemical families (family of calcium and magnesian chloride sulphates which represents 95% and family of calcium and magnesian bicarbonates which represents 5%). From the chemical facies point of view, the ground and surface waters of the Yaya district are mainly characterized by chemical facies of the magnetic sulfate and chlorinated-sulfated calcium and magnesian type;

- From a quality point of view, the comparative analysis of the physico-chemical parameters admissible by the WHO and of ground and surface water has shown that the good potability of these waters is called into question by the presence of certain elements such as total iron (Fe_{tot}), hexavalent chromium (Cr^{6+}), lead (Pb^{2+}) and aluminium (Al^{3+}), the levels of which sometimes exceed the values of maximum admissible concentrations for drinking water defined by the WHO. In addition to these elements, there are also fluorine and nitrates, which, although they are present at levels acceptable to WHO standards, can cause adverse health effects in the long term for the population of Yaya District.

Finally, the determination of the aggressive character of the ground and surface waters of Yaya district from the Langelier and Ryznar stability index, allowed us to know that the ground and surface waters of Yaya district are aggressive and very strongly corrosive, i.e. they dissolve calcium carbonate and can attack the metallic equipment of the boreholes.

REFERENCES

[1] **Moudzika Loubaki, H. B. (2017).** Evolution des caractéristiques physico-chimiques et étude de l'agressivité des eaux souterraines et de surface du district de Yaya (Département du Niari). Mémoire de Master de Géosciences, Faculté des Sciences et Techniques, Univ. Marien NGOUABI (Brazzaville), 73 p.

[2] **Moukolo, N., Samba-Kimbata, M. J., Mpounza, M., Nzalabaka, J., Maziezoula, B. & Ossete, J. M. (1992).** Hydrogéologie du Congo. Bulletin du BRGM n°210, 125 p.

[3] **Dadet, P. (1969).** Notice explicative de la carte géologique de la République du Congo au 1/500.000, zone comprise entre les parallèles 2° et 5° sud. Brazzaville : BRGM rapport, 103p.

[4] **Gerard, G. (1958).** Carte géologique de l'Afrique équatoriale française au 1/2000000. Notice explicative. Publ. Dir. Mine et Géo. A.E.F., Brazzaville, 198 p.

[5] **Chevallier, L., Makanga, J.F. & Thomas, R.J. (2002).** Notice explicative de la Carte géologique de la République Gabonaise à 1/1000000. Editions DGMG Gabon, 195 p.

[6] **Boudzoumou, F. (1986).** La chaine ouest-congolienne et son avant-pays au Congo : Relations avec le Mayombien ; Sédimentologie des séquences d'âge protérozoïque supérieur. Thèse de Doctorat de 3ème cycle, Univ. D'Aix Marseille III. pp. 21-42.

[7] **Thieblemont, D., Castaingt, C., Billa, M., Bouton, P. & Preant, A. (2009).** Notice explicative de la carte géologique et ressource minérales de la République Gabonaise (Libreville), (384), pp. 18-84.

[8] **Vennetier, P. (1966).** Géographie du Congo-Brazzaville. Centre d'Enseignement Supérieur de Brazzaville, GAUTHIER-VILLARD-Paris. 174 p.

[9] **Boudzoumou, F., Sounga, J.D. & Moussiessie, J. (2005).** Lithostratigraphie : Le groupe des diamictites et grés inferieurs ; bases du Super-Groupe de l'Ouest-Congo. Ann. Univ. M. NGOUABI, Vol. (6, 1), pp. 85-90.

[10] **Van Daalhoff, H. (1966).** Mission paléogéographique du Bouenzien. Recherche des gisements stratiformes. Rapp. BRGM. Inédit, BRA-65-A-8.

[11] **Boineau, R. (1957).** La série du Bouenzien dans la coupure Sibiti-Ouest. Publ. Dir. Mine et Géol. A.E.F., n° 8, 1957, pp. 17-20.

[12] **Boudzoumou, F. & Trompette, R. (1988).** La chaine panafricaine Ouest-Congolienne au Congo (Afrique Equatoriale) : Un socle polycyclique charrié sur un domaine subautochtone formé par l'aulacogène du Mayombe et le bassin de l'Ouest-Congo. Bulletin de la Société Géologique de France, Vol. 6, pp. 889-896.

[13] **Ahmat Mahamat, H. (2014).** Caractérisation hydrogéologique de la nappe exploitée dans le district de Yaya : Géométrie de l'aquifère. Mémoire de Master de Géosciences, Faculté des Sciences et Techniques, Univ. Marien NGOUABI (Brazzaville), 47p.

[14] **Seguin, J.J. (2005).** Projet Réseau SIG-Afrique Carte hydrogéologique de l'Afrique à l'échelle du 1/10000000, BRGM/RP-54404-FR. 66 p.

[15] **Kirchmer, J.C. (1983).** Quality control in water analyses. Environmental Science and Technology, 17 (4), pp. 178-181.

[16] **Fetter, C.W. (1994).** Applied hydrogeology. Prentice Hall Inc., New Jersey (USA), 691 p.

[17] **Rodier, J. 1996 (p12)**. L'analyse de l'eau, eaux naturelles, eaux résiduaires, eaux de mer. Edition Dunod, 1434 p.

[18] **OMS/WHO (2004).** Guidelines for drinking-water quality third edition, 504 p.

[19] Jordana, S. & Batista, E. (2004). Natural groundwater quality and health. Geologica Acta, Vol. 2, n°2, pp. 175-188.

[20] OMS/WHO (2000). Directives de qualité pour l'eau de boisson. 2nd Ed., Vol. 2, Critères d'hygiène et documentation à l'appui, 1050 p.

[21] Brouwer, I.D., De Bruin, A., Dirks, O.A. & Hautvast, J. (1988). Unsuitability of WHO guidelines for fluoride concentration in drinking water in Senegal. Lancet, 1, pp. 223-225.

[22] Kothari, N. (1988). Groundwater, iron and manganese: an unwelcome trio. Water/Engineering & Management, Vol.135, n°2, pp. 25-26.

[23] Abdoulaye Demba, N., Mohamed, O. & Khalid, I. (2013). Contribution à l'étude de l'origine du plomb contenu dans les effluents de la Step utilisés en agriculture dans le périmètre maraicher du SEBKHA (Mauritanie). Larhyss n°12, 8 p.

[24] Bakalowicz, M. (1979). Contribution de la géochimie des eaux à la connaissance de l'aquifère karstique et de la karstification. Doctorat d'Etat, Univ. Pierre et Marie Curie, Paris VI. 343 p.

[25] Banton, O., Bangoy, L.M., Chevalier, S., Houenou, P., Lafrance, P. & Rivard, C. (1997). Hydrogéologie : Multiscience environnementale des eaux souterraines. Presses de l'Université du Québec/AUPELF, 460 p.

[26] Ravindra, K. & Garg, V.K. (2007). Hydrochemical survey of groundwater of Hisar City and assessment of defluoridation methods used in India. Environ Monit Assess, n°132, pp. 33-43.

Use of De-Aluminated Metakaolin Waste as A Supplementary Cementitious Material in Mortars

Dr. Enas A.A. Khattab
Assoc. Professor, Building Material and Quality Control, Research Institute, Housing & Building National Research Center.

ABSTRACT

Supplementary cementitious materials have been widely used all over the world in concrete due to their economic and environmental benefits. Mineral admixtures such as fly ash and silica fume are more commonly used as Supplementary cementitious materials. Metakaolin, other type of pozzolan, produced by calcination at 650-800 ◦C. This paper presents the results of an experimental investigations carried out to find the suitability of using de-aluminated metakaolin waste obtained from Aluminum Sulphate co. of Egypt production factory through the extraction of aluminum as Supplementary cementitious materials. An experimental program was designed to study the effect of different dosages of De-Aluminated Metakaolin on the flowability and compressive strength of mortars, microscope scanning was carried out for some tested samples containing different percentage of De-Aluminated Metakaolin. De-Aluminated Metakaolin was used as replacement and addition of cement content. The used De-Aluminated Metakaolin had two degrees of fineness. The results of De-Aluminated Meta-Kaolin mixes were obtained and compared with those of mixes contain metakaolin from the same source. The results show that using of De-Aluminated Metakaolin with degree of fineness closed to cement fineness as addition of cement content has a significant effect on compressive strength of mortar closed to those of mixes with metakaolin with higher fineness (twice the cement fineness). The increase in compressive strength were 14% and 13% compared with control mix for De-Aluminated Metakaolin and metakaolin dosages of 15% and 10%, respectively.

KeyWords: De-Aluminated, Meta-Kaolin, Mortars, Cement, Addition, Replacement.

I. INTRODUCTION

Meta-Kaolin is a pozzolanic material it is a thermally activated aluminosilicate material with high pozzolanic activity comparable to or exceeded the activity of silica fume. When cement is partially replaced with metakaolin, it reacts with byproduct calcium hydroxide and results in extra C-S-H gel. For strength development in cement and cement based concrete C-S-H gel is the sole cause. The several researchers have studied on various parameters by replacing the cement by metakaolin which includes fineness, mineral composition, workability, various strengths of cement mortars and concrete.

Dinaker et al [1] study the effect of incorporating metakaolin on the mechanical and durability properties of high strength concrete for a constant water / binder ratio of 0.3. metakaolin mixtures with cement replacement of 5, 10 and 15 % were designed for high strength and high performance concrete. The optimum replacement level of cement by metakaolin was 10%, which gave the highest compressive strength in comparison to that of other replacement level.

Memduh nas and sirin kurbetci [2] investigated the possible effects of metakaolin on strength properties of concrete. concrete mixtures were produced by substituting cement with metakaolin

0,5,10 and 20% by weight. The optimum replacement level of cement by metakaolin was 20%, which gave both the highest compressive strength and the highest flexural strength in comparison to that of other replacement level.

Guo et al [3] studied the compressive behavior of nano metakaolin cement mortar mixed with other pozzolanic materials. The results show that the compressive strength of nano metakaolin cement mortar mixed with granulated blast furnace, slag, fly ash, and attapulgite clay were 33.38%, 17.65%, and 6.45 higher than that the ordinary mortars, respectively.

Mohamed et al [4] show that the optimum dosage of metakaolin as a partial cement replacement was 15% to 20% at water binder ratio of 0.4. it achieved an increase in compressive strength by 25% which compared to control mixes.

Mayuri and Pawade [5] introduced a review for influence of metakaolin in concrete mixture. According to These review, use of 25% metakaolin in replacement of cement increased strengths of all basic properties.

Farazad et al introduced [6] a review of properties of metakaolin concrete. According to These review, relatively finer and higher pozzolanic metakaolin as a partial replacement of cement produces pore structure modification, reduces porosity and pore size refinement in the hardening pastes and concretes.

H. Moselhy [7] investigated the possibility of using dealuminated metakaolin as cementatious materials in concrete slump and compressive strength were measured for mixes containing 0, 5, 10 and 15% dealuminated metakaolin as replacement of cement. Results showed that slump steadily increasing with increase percentage of dealuminated metakaolin and 5% replacement increased the compressive strength by 2.8%.

A. M. K. Abdelalim et.al. [8] studied the suitability of replacing Portland cement by dealuminated calcined kaolin waste and dealuminated samples treated with lime solution. The effect of replacement on setting time, flowability, rate of flowability loss and strength of mortars for replacement ratios 0, 5, 10, 15 and 20% were measured. Results showed that the DKut accelerate the setting time and hardly affect the flowability loss and 10% replacement improve compressive and tensile strength of mortars

II. RESEARCH PROGRAM

The experimental program was divided into two phases based on the fineness of the de-aluminated metakaolin. Through phase one, the used De-Aluminated Metakaolin has fineness of 2000 cm^2/gm. (as delivered by the factory). Twenty mortar mixes were cast using De-Aluminated Metakaolin with 5, 10, 15, 20, 25, 30, 35, 40, 45 and 50% replacement/addition ratios of cement content. In the second phase, the delivered De-Aluminated Metakaolin was grinded to achieve fineness of 3750 cm^2/gm. Fourteen mortar mixes were cast with De-Aluminated Metakaolin of 5,10,15,20,25,30 and 35% replacement/addition ratios of cement content. Based on the compressive strength results, four selected mixes from phase two were compared with mixes contained metakaolin has fineness of 6400 cm^2/gm (from the same source) with the same replacement/addition ratios of 10, 15, 20 and 25 % of cement content.

The proportions by mass of the control mix was one part of the cement, three parts of fine aggregate. Each batch for three test specimens consisted of (450 ± 2) g of cement, (1350 ± 5) g of sand and different water contents were used to achieve constant flow of (180 -190 mm). Table 1and table 2 represented the mixes proportion ratios of the mortars mixes.

Nine cubic specimens with 50 mm side length were prepared for every mixture to measure the compressive strength at ages of 3, 7 and 28 days. Micro structure analysis was performed using scanning electron microscope (SEM) for the selected mixes.

III. MATERIALS PROPERTIES

Natural siliceous sand, ordinary Portland cement (OPC), tap drinking water and De-Aluminated Meta-Kaolin were used in this work. Testing of these materials was carried out according to Egyptian Standard Specifications and the ASTM standards. The cement used in this investigation was "Egyptian Ordinary Portland Cement" which is manufactured locally and complies with the standard

specifications. The chemical analysis as well as the physical properties of the used cement as determined by laboratory tests showed its suitability for concrete work. De-Aluminated MetaKaolin was used as replacement and addition of cement content as supplementary cementitious material. The used De-Aluminated MetaKaolin was brought from the factories of Aluminum Sulphate Company of Egypt with specific surface area 2000 cm^2/gm for phase one mixes while in phase two, De-Aluminated MetaKaolin was grinded to specific surface area 3750 cm^2/gm. The chemical compositions of the cement, Metakaolin was brought from the factories of Aluminum Sulphate Company of Egypt with specific surface area 6400 cm^2/gm. De-Aluminated metakaolin and metakaolin were specified in Table 3 .X-ray diffraction analysis was performed on the metakaolin and the diffraction pattern of De-Aluminated meta-kaolin was shown in Figure 1. The crystalline phases of De-Aluminated metakaolin are composed of quartz, micas and anatase. A dome-like region between 2θ = 20-30 shows the amorphous phase resulting from the applied heat treatment of kaolinite. This dome shaped amorphous structure is a clear indication that De-Aluminated meta-kaolin reaches a glassy and results in a pozzolanic character.

IV. TEST RESULTS AND DISCUSSION

Results of phase one indicated that using De-Aluminated Metakaolin of 2000 cm^2/gm specific surface area significantly decreased the compressive strength whether as replacement or addition ratio of cement as illustrated in Table 4. That could be attributed to the low specific surface area of De-Aluminated Metakaolin waste which reduced the reaction surface area and increased the water demand to reach the same flow.

Table 5 showed that increasing De-Aluminated Metakaolin specific surface area up to 3750 cm^2/gm led to enhancement of compressive strength when used as addition ratio from cement in mortar mixes. Adding ratios of 5% does not affect the compressive strength while adding 10, 15 and 20% ratios increased compressive strength by 10, 14 and 7%, respectively. Adding ratios higher than 20% decreased the compressive strength. Using of De-Aluminated Meta-Kaolin with degree of fineness closed to cement fineness as an addition of cement improved the concrete microstructures involving micro effect and chemical effect (pozzolanic reaction). See figure 2

On the contrary, replacing cement with De-Aluminated Metakaolin significantly decreased the compressive strength, as shown in figure 3. That could be explained as a result of a clinker dilution effect. The dilution effect is a result replacing a part of cement by the equivalent quantity of metakaolin.

It was observed that adding De-Aluminated Metakaolin reduced the strength gain at early ages of 3 and 7 days. Compressive strength at 3days of mixes with De-Aluminated Metakaolin developed about 25-35% of the 28 days strength while cement mortars at the same age developed 67% of the target strength. At age of 7 days, mixes with De-Aluminated Metakaolin developed 54-59% of the target strength while cement mortars got 75% of the target strength.

From table 6, adding metakaolin with 10% of cement content increased the compressive strength by 13% while adding metakaolin with higher ratios 15, 20 and 25% didn't present any effect on compressive strength. As in figure 4, comparing the effect of adding metakaolin or de-aluminated metakaolin on compressive strength it could be found the de-aluminated metakaolin presented better enhancement of compressive strength due to

the increase of the SiO_2 content in dealuminated metakaolin, higher SiO_2 content improved the pozzolanic action.

Mixes With De-Aluminated MetaKaolin As Addition of Cement Content					Mixes With De-Aluminated MetaKaolin As Replacement of Cement Content				
Mix	cement (gm)	De-Aluminated MetaKaolin		Water (gm)	Mix	cement (gm)	De-Aluminated MetaKaolin		Water (gm)
		% of addition	(gm)				% of replacement	(gm)	
C	450	0	0	225					
DA2		5	22.5	225	DR2	427.5	5	22.5	235
DA3		10	45	228	DR3	405	10	45	245
DA4		15	67.5	230	DR4	382.5	15	67.5	250
DA5		20	90	235	DR5	360	20	90	255
DA6		25	112.5	255	DR6	337.5	25	112.5	260
DA7		30	135	268	DR7	315	30	135	275
DA8		35	157.5	275	DR8	292.5	35	157.5	283
DA9		40	180	285	DR9	270	40	180	290
DA10		45	202.5	300	DR10	247.5	45	202.5	295
DA11		50	225	310	DR11	225	50	225	298

Table 1: Phase one mix proportion ratio

Mixes With De-Aluminated MetaKaolin As Addition of Cement Content					Mixes With De-Aluminated MetaKaolin As Replacement of Cement Content				
Mix	cement (gm)	De-Aluminated MetaKaolin		Water (gm)	Mix	cement (gm)	De-Aluminated MetaKaolin		Water (gm)
		% of addition	(gm)				% of replacement	(gm)	
C	450	0	0	225					
DA2		5	22.5	228	DR2	427.5	5	22.5	240
DA3		10	45	232	DR3	405	10	45	252
DA4		15	67.5	235	DR4	382.5	15	67.5	260
DA5		20	90	242	DR5	360	20	90	265
DA6		25	112.5	260	DR6	337.5	25	112.5	270
DA7		30	135	270	DR7	315	30	135	275
DA8		35	157.5	280	DR8	292.5	35	157.5	283

Mixes With De-Aluminated MetaKaolin As Addition of Cement Content					Mixes With De-Aluminated MetaKaolin As Replacement of Cement Content				
Mix	cement (gm)	De-Aluminated MetaKaolin		Water (gm)	Mix	cement (gm)	De-Aluminated MetaKaolin		Water (gm)
		% of addition	(gm)				% of replacement	(gm)	
C	450	0	0	225					
DA2		5	22.5	225	DR2	427.5	5	22.5	235
DA3		10	45	228	DR3	405	10	45	245
DA4		15	67.5	230	DR4	382.5	15	67.5	250
DA5		20	90	235	DR5	360	20	90	255
DA6		25	112.5	255	DR6	337.5	25	112.5	260
DA7		30	135	268	DR7	315	30	135	275
DA8		35	157.5	275	DR8	292.5	35	157.5	283

Table 2: Phase two mix proportion ratio

Table 3: The chemical composition

DA9		40	180	285	DR9	270	40	180	290
DA10		45	202.5	300	DR10	247.5	45	202.5	295
DA11		50	225	310	DR11	225	50	225	298

Chemical Compositions	**Cement %**	**De-Aluminated Metakaolin**	**Metakaolin**
SiO_2	21.0 %	78.3	52.83
Al_2O_3	6.10 %	6.53	41.3
Fe_2O_3	3.00 %	0.66	1.38
CaO	61.5 %	0.37	0.28
MgO	3.8 %	-	-
So_3	2.5 %	2.53	0.95
TiO2	-	3.92	0.87
Loss ignition %	1.5 %	7.23	2.1

Table 4: Phase one Experimental Results

Mixes With De-Aluminated MetaKaolin As Addition of Cement Content					Mixes With De-Aluminated MetaKaolin As Replacement of Cement Content				
Mix	Flow (mm)	Compressive Strength (MPa)			Mix	Flow (mm)	Compressive Strength (MPa)		
		3 days	7 days	28 days			3 days	7 days	28 days
C	185.5	31.2	35.4	46.8					
DA2	182.5	19.5	30.0	33.5	DR2	180	16.3	21.3	39.7
DA3	186.5	15.6	28.0	29.1	DR3	188	14.2	25.3	34.6
DA4	183.5	13.5	23.8	26.1	DR4	188	9.6	22.0	30.3
DA5	182.5	16.4	18.1	20.6	DR5	188	10.6	13.1	28.2
DA6	182.5	7.7	12.9	17.2	DR6	184.5	8.3	14.2	26.6
DA7	181	12.1	15.9	17.3	DR7	187.5	6.6	11.4	13.7
DA8	183	10.6	14.4	18.1	DR8	187	6.8	9.5	10.8
DA9	182	9.6	12.9	14.1	DR9	189	6.5	10.0	13.9
DA10	182.5	8.8	12.4	17.9	DR10	185	8.9	12.2	14.9
DA11	184	11.8	12.6	18.2	DR11	188	8.7	13.3	16.5

Table 5: Phase two Experimental Results

Mixes With De-Aluminated MetaKaolin As Addition of Cement Content					Mixes With De-Aluminated MetaKaolin As Replacement of Cement Content				
Mix	Flow (mm)	Compressive Strength (MPa)			Mix	Flow (mm)	Compressive Strength (MPa)		
		3 days	7 days	28 days			3 days	7 days	28 days
C	183.5	31.2	35.4	46.8					
DA2	184.5	20.4	32.5	45.0	DR2	180	16.7	26.3	43.2
DA3	183.5	18.4	30.6	51.6	DR3	186	14.5	21.4	37.2
DA4	184	15.2	28.7	53.4	DR4	186.5	14.2	15.9	34.3
DA5	184.5	13.4	27.4	50.2	DR5	187.5	10.3	14.9	30.2
DA6	183.5	12.0	25.9	42.0	DR6	185.5	10.7	13.9	27.4
DA7	186	9.9	21.4	39.4	DR7	185	10.7	13.5	26.4
DA8	184	9.2	16.2	32.8	DR8	180.5	9.8	11.2	24.5

Table 6: The Experimental Results of MetaKaolin Mixes

Mixes With MetaKaolin As Addition of Cement Content					Mixes With MetaKaolin As Replacement of Cement Content				
Mix	Water (gm)	Flow (mm)	Compressive Strength (MPa)		Mix	Water (gm)	Flow (mm)	Compressive Strength (MPa)	
			7 days	28 days				7 days	28 days
C	225	183.5	35.4	46.8					
MA3	230	180.5	34.4	52.9	MR3	240	184	38.3	46.1
MA4	235	181.5	39.5	46.0	MR4	245	183	28.2	42.4
MA5	245	182.5	33.4	45.6	MR5	245	182	28.7	41.9
MA6	265	185	32.0	45.5	MR6	255	180	34.3	44.0

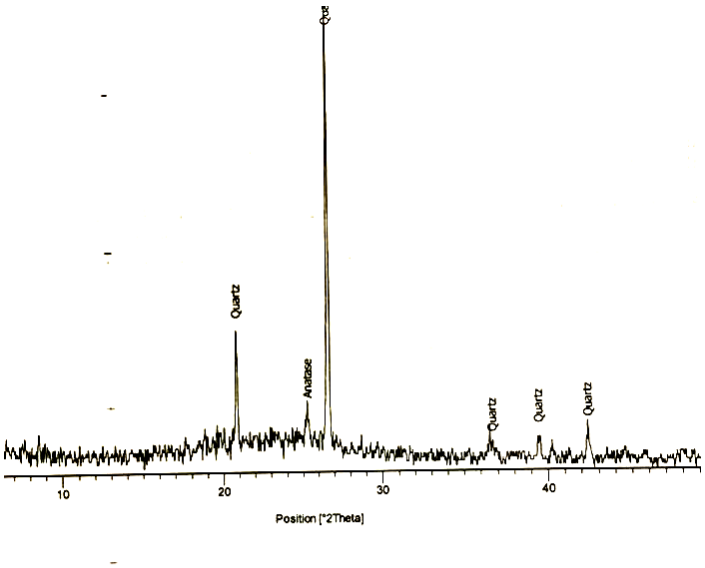

Compound Name	Chemical Formula
Quartz	Si O2
Anatase	Ti O2

Figure 1: X-ray diffraction analysis of De-Aluminated meta-kaolin

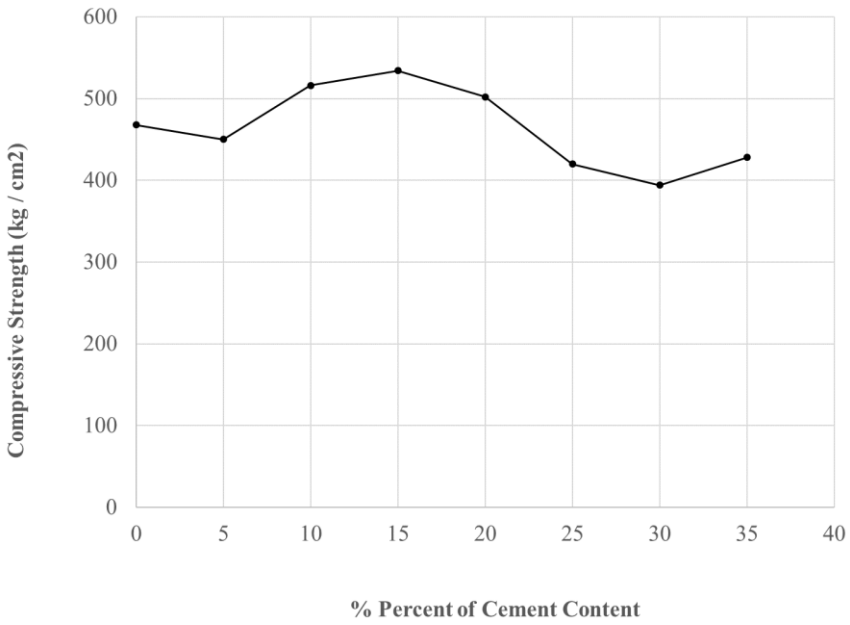

Figure 2: 28 days compressive strength of De-Aluminated Metakaolin mixes with fineness of 3750 cm2 / gm as addition

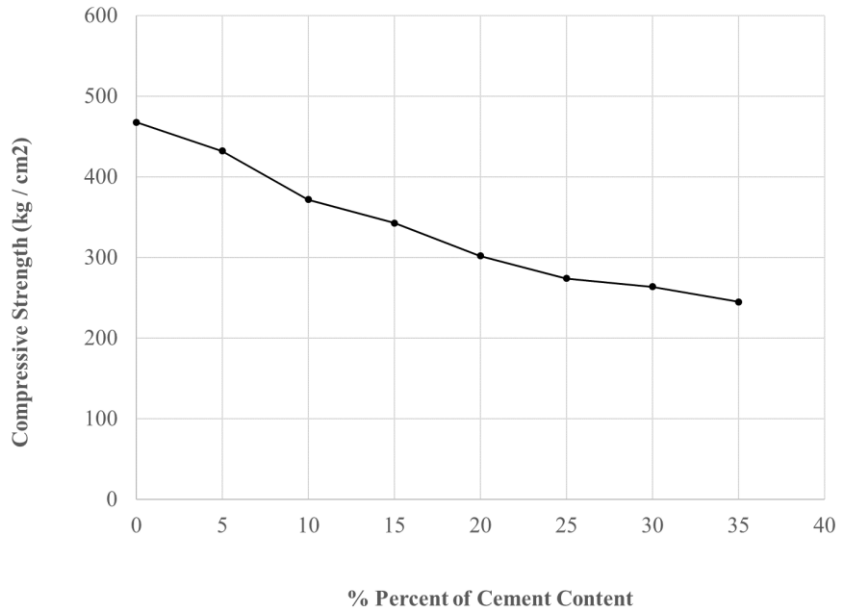

Figure 3: 28 days compressive strength of De-Aluminated Meta-Kaolin mixes with fineness of 3750 cm^2 / gm as replacement

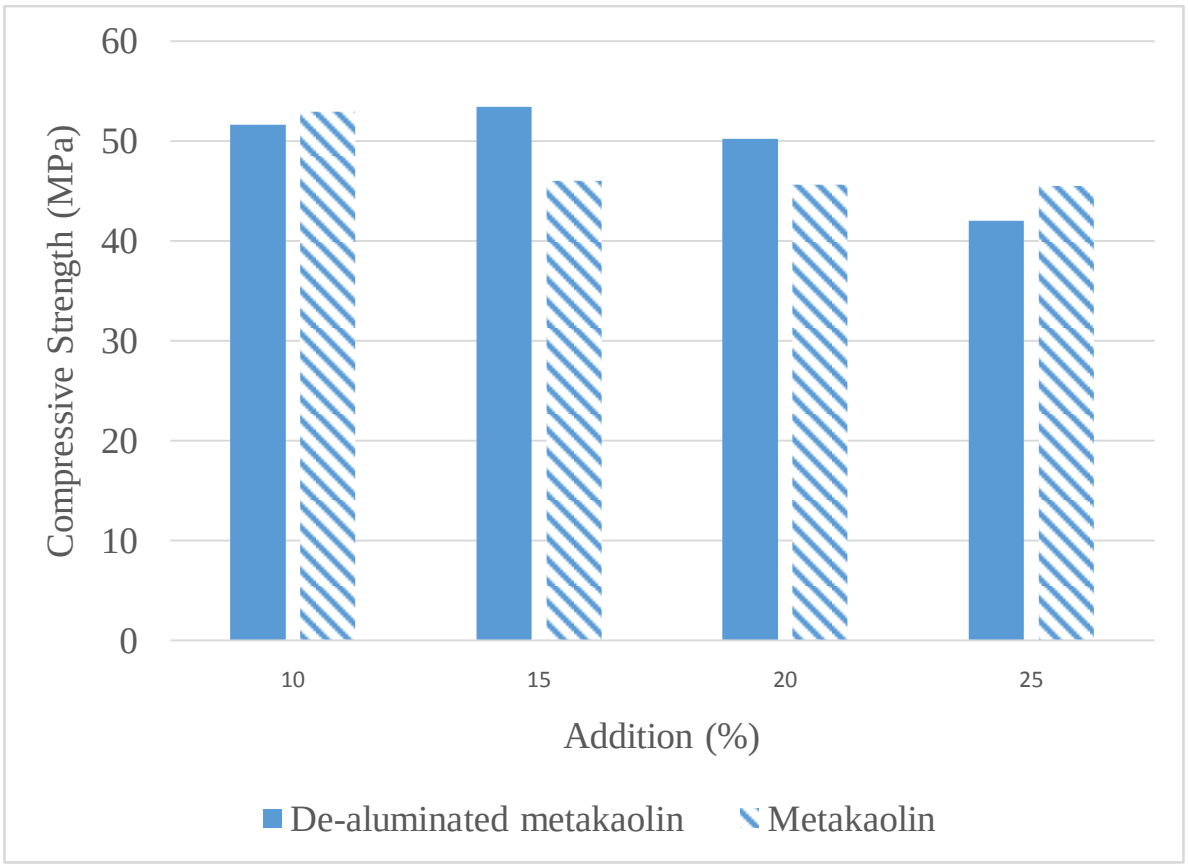

Figure 4: Comparison between 28 days compressive strength of adding De-Aluminated Metakaolin and Metakaolin

V. SEM results

Figure 5 present the microstructure for some mixes containing different adding percentage of de-aluminated metakaolin. It was evident that, the physical action of the pozzolans generally provides a denser, more homogeneous and uniform pastes.

The addition of the Pozzilanic material like de-aluminated metakaolin to Portland cement OPC generally increases its mechanical strength and durability when compared to the blank paste. It was noticed that the control sample had the lowest compressive strength, while, increasing the percentage of the de-aluminated metakaolin up to 15% generally increase the compressive strength.

This may be due to the additional hydration of un-hydrated cement grains. The increase of compressive strength of blended cement pastes may be due to the pozzolanic reaction of de-aluminated metakaolin as a rich silica source with free lime that gives the availability of transformation of calcium hydroxide to extra calcium silicate hydrate deposited in the pores. Cement matrix with higher volumes of gel-like hydration products, and lower crystalline calcium hydroxide contents has improved the compressive strength. This is in turn has an active contribution in increasing the bonding forces between particles resulting in the increase of compressive strength of the blended compounds. Also, the increase of compressive strength of blended cement pastes may be due to the interfacial bonds

It was also noted that increasing the percentage of the de-aluminated metakaolin more than 15% decrease the compressive strength. This may due to the weakened bonds between the contents due to un-sufficient OPC grains as a bonding media for the contents resulting in lowering the compressive strength. It could be noticed that the pore structure coarsening intensified as the formation of micro-cracks.

It could be concluded that an about 15% de-aluminated metakaolin replacement, the fine particulates have facilitated the most efficient hydration processes and hence induced an increase in the compressive strength of the blended cement

paste.

0% dealuminated metakaolin

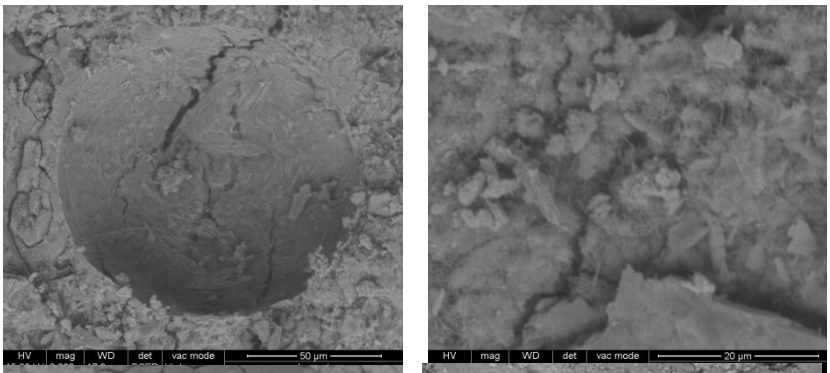

10%

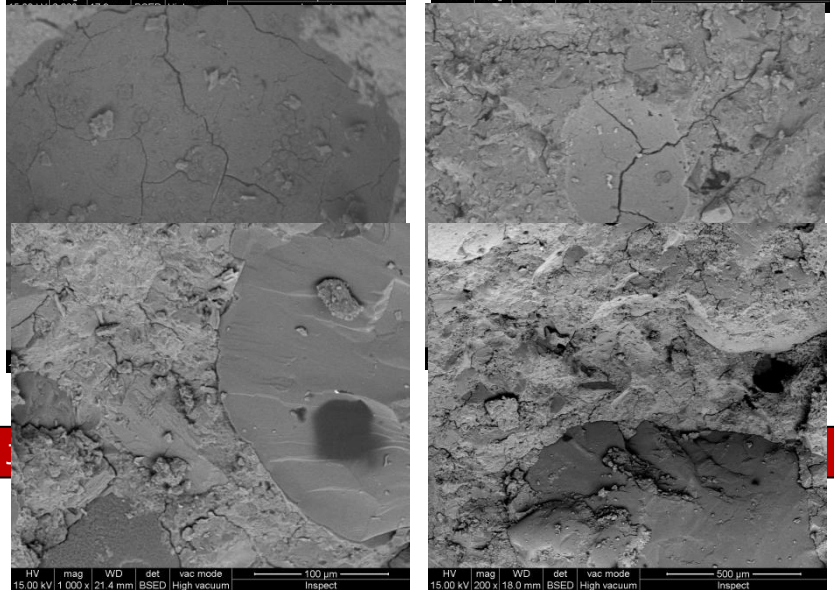

15%

20%

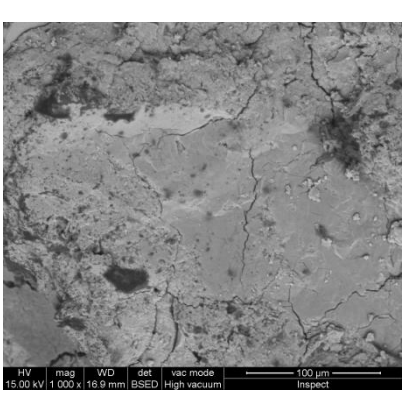

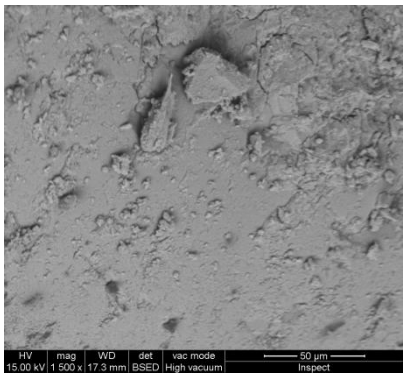

Figure 5: microstructure for specimens containing different adding percentage of dealuminated metakaolin

VI. CONCLUSIONS

From the analysis and discussion of the test results obtained from this research, the following conclusions can be drawn:

- Using De-Aluminated Metakaolin with specific surface area 3750 cm^2 / gm acted in similar manner as Metakaolin with specific surface area 6400 cm^2 /gm.
- Water binder ratio increase with the increase of De-Aluminated Metakaolin or Metakaolin to achieve constant flow.
- De-Aluminated Metakaolin must be having at least degree of fineness closed to cement fineness to improve the concrete microstructures involving micro effect and chemical effect (pozzolanic reaction).
- The optimum addition level of cement by De-Aluminated Metakaolin were 10 % and 15 % respectively, which gave the highest compressive strengths in comparison that of other addition levels, this was due to the dilution effect of partial cement addition.

REFERENCES

1- Dinakar, P., Pradosh, K.S., and Sriram, G., "Effect of Metakaolin Content On the Properties of High Strength Concrete", International Journal of Concrete Structures and Materials, V. 7, No. 3, 2013, pp.215-233.
2- Memduh nas and sirin kurbetci "Durability Properties of Concrete Containing Metakaolin", Journal of Advances in Concrete Construction, V. 6, No. 2, 2018, pp.159-175.
3- Guo Xiaoyu, Fan yingfang, and Luan Haiyang, "The Compressive Behavior of Cement Mortar with The Addition of Nano Metakaolin", Journal of nanomaterials and nanotechnology, V. 8, 2018.
4- Mohamed, M.R., Abdl Rahman, M., and Mohamed, S.E., "Effect of Local Metakaolin On Properties of Concrete and Its Sulphuric Acid Resistance", Journal of Engineering Sciences, Assiut, V. 43, No. 2, March 2015, pp.183-199.
5- Mayuri, A.C., Pawade, P.Y., "Influence of Metakaolin in Concrete Mixture: A Review", IJES Journal, ISSN 2319-1813, pp.37-41.

6- Farazad, K.M., Rasiah, S.R. and Vute, S., "Properties of Metakaolin Concrete – A Review", Int. Conference on Sustainable Structural concrete, 15-18 Sept 2015, pp.157-168.
7- H. Moselhy, "Effect of dealuminated kaolin waste on slump and compressive strength of ordinary Portland cement concrete", International journal of chemical engineering, volume 10, Number 2 (2018)
8- A. M. K. Abdelalim, H. Y. Ghorab, G. E. Abdelaziz and M. S. Elsayed, "Dealuminated kaolin as a cement replacement materials", Journal cement Wapno Beton, 3rd issue, January 2010.

Implementation of statistical methods to the comparative study of heavy minerals of the Cover Formation and its bedrock in the Pointe-Noire and Brazzaville sectors (Republic of Congo)

Miyouna T.[1,*], Essouli. O. F.[1], Malanda Nimy E. N[1],Boudzoumou F.[1,3],Kendé M.[1],Mokono-Mboko C.[1], Sow E. H.[2]

[1]*Marien Ngouabi University, Facultyof Sciences and Technology, Department of Master, Laboratoryof Geosciences, P.O. Box: 69, Brazzaville, Republic of Congo*
[2]*Cheikh Anta DiopUniversity of Dakar, Faculty of Sciences and Technology, Department of Geology, Laboratory of sedimentologyand Biostratigraphy, P.O Box: 5005, Dakar-Fann, Republic of Senegal*
[3]*Research Institute in Exact and Natural Sciences, Department of Geosciences, P.O. Box: 2400, Brazzaville, Republic of Congo*

ABSTRACT

The comparative study of the heavy minerals of the Cover Formation and its bedrock by statistical methods was carried out in Pointe-Noire and Brazzaville in order to understand its nature, origin, and relationship with its bedrock. The study shows that the Cover Formation contains a constant and homogeneous paragenesis of heavy minerals, which distinguishes it qualitatively and quantitatively from its bedrock. These heavy minerals come from the same distant source, containing mainly metamorphic rocks of green shale and amphibolite grades, secondarily magmatic and sedimentary or metasedimentary rocks. These heavy minerals have been transported by the wind after sometimesseveral sedimentary recycles. The Cover Formation hasan aeolian, it is not the product of *in-situ*weathering of its bedrock. So that, it must be stratigraphically separated from its bedrock as proposed by Thiéblemont et *al.* (2009) in Gabon.

Keywords: Heavy minerals, stone line, aeolian, CoverFormation, bedrock, Congo

I. Introduction

The Cover Formation is the yellow ochre sand that overlies all ancient formations in Congo, of Archean, Proterozoic, Neoproterozoic, Paleozoic, Mesozoic and Cenozoic age through a gully unconformity materialized by a polygenic or monogenic, simple or complex, autochthonous or allochthonous stone line, either by a palaeosolof Lousséké or ferralsol type **[1]; [2];[3]**. It stretches from Cameroon to Namibia through Gabon, the Republic of Congo, the Democratic Republic of Congo and Angola **[2]; [3]; [4]; [5]; [6]; [7]; [8];[9]; [10]; [11]; [12]; [13]; [14], [15]**. This yellow ochre sand is subject to several controversies. It is considered to be either the product of *in-situ*weathering of its bedrock, homogenized by termites **[8];[9]; [13]** or an allochthonous deposit of aeolian origin **[1]; [2]; [3]; [14]; [15]**. In the Congolese Atlantic coastal basin, for example, this yellow sand of the Cover Formation was associated withthe upper unit of the “Série des Cirques **[4]; [6]; [8];[9]** of Lower Miocene age **[16]**. On other and, in the Series of “Plateaux Téké” it forms the upper unit (Ba2)**[17]**. Since the work carried out by Thiéblemont **[14];[15]** in Gabon, this yellow ochre sand is considered as a stratigraphicalFormation, called “Cover Formation” or “Cover Horizon”, belonging to the Stone line Complex **[1]**. The age of the Cover Formation obtained by radiometric dating (^{14}C) ranges from 3000 years B.P. to 2000 years B.P. **[1]; [14]; [15]**. These ages are however rejected by Schwartz **[18]**.In Republic of Congo, the Cover Formation is less studied.Most of the studies are old, although recent

geological map work has studied a few sites containing this Formation **[1]**. This work studies and compares the heavy minerals contained in the Cover Formation and its bedrock, in order to determine the origin of its sediments and to conclude on its allochthony or autochthony. The samples used come from three fairly distant profiles in which the Cover Formation and his bedrock are well individualized. These are the Diosso profile located in the Kouilou department, the profiles of the "Pont du Djoué" cliff and "Main Bleue" both located in southern Brazzaville. The Figure 1 situates and locates them on the geological map of Dadet**[6]**. Due to field difficulties, the Cover Formation was not sampled in the Diosso profile, but it was sampled at Malélé where it is more accessible and thicker.

II. Material and Methodology

2.1. Situation and geological context of the studied profiles

The profile of Diosso is located in the Congolese Atlantic coastal basin of Mezo-Cenozoic age **[16]; [19]**. The cliff of the "Pont du Djoué" is located in the Palaeozoic Inkisi basin **[20]; [21]** and the profile of "Main bleue" is located in the Meso-Cenozoic basin of Congo**[1]; [22]** (**Figure 1**).

The Congolese Atlantic coastal basin located in the western Mayombemountain, originated in the Jurassic (Neocomian) period following the break-up of Gondwana and its separation into South America and the West Africa-Arabia to the east.

The evolution of the Congolese coastal sedimentary basin comprises three phases of sedimentary construction which correspond to three phases of tectono-dynamic evolution**[23]** described as follows: the ante-salt phase (which begins at the end of the Jurassic, but developed mainly from the Barremian to the Lower Aptian); the salt phase (which reflects the beginning of the marine transgression and ends the rifting stage); and the post-salt phase (which is the terminal sedimentary unit of the coastal basin). At the Lower Miocene, the fluvio-deltaic "Series des Cirques" covers the marine formations. The "Série des Cirques" is mainly composed of silico-clastic sediments **[24]**, structured in finning-up elementary sequences. The yellow ochre sands of the "Cover Formation essentially are essentially composed of thin quartz. They are underlain by a laterite and a stone line in the "Série des Cirques" of Diosso.

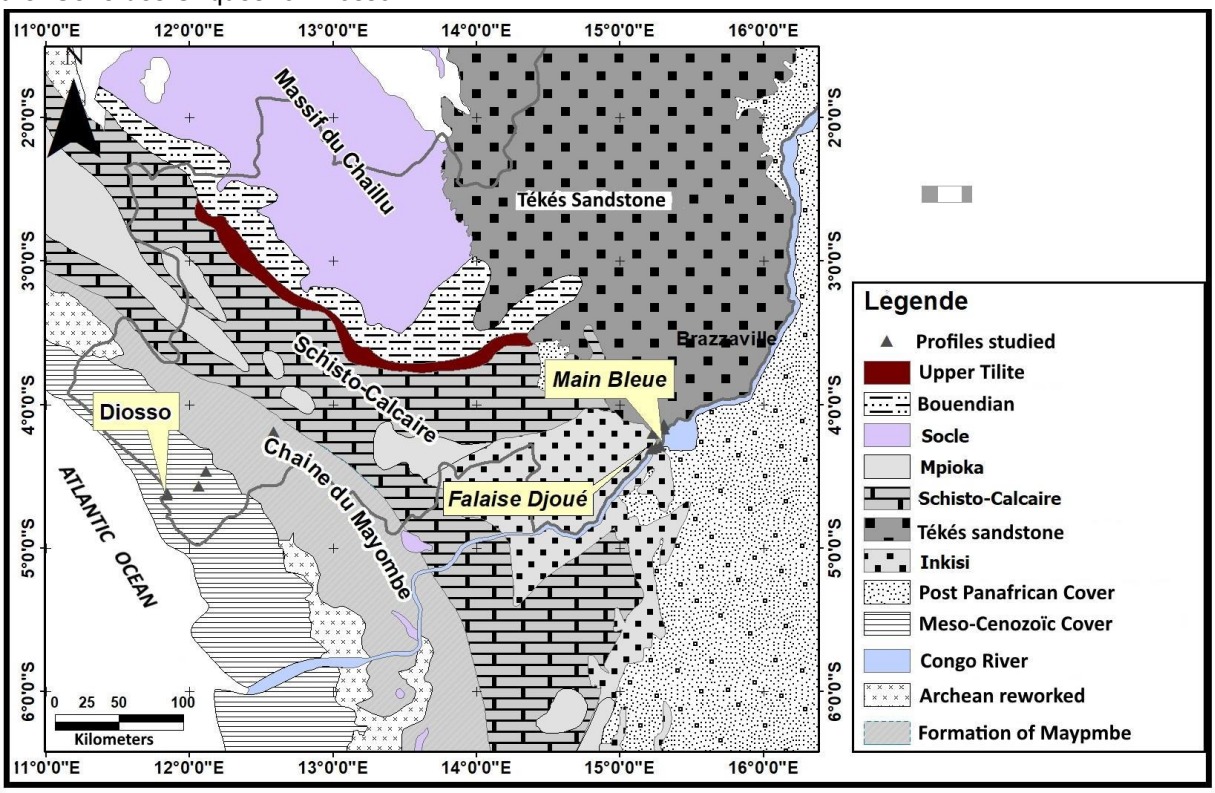

***Figure 1**. Situation and location of the different studied profiles on the geological map of the Republic of Congo* **[6]**

The Profile of "Pont du Djoué" cliff is essentially made of red ochre sandstones of Inkisi Group which is part of the Lindian Supergroup of Combro-Ordovician age **[1]**. The age of the Inkisi Formation, obtained from the youngest detrital zircons, varies between 518±18 Ma and 558±56 Ma **[20]; [21]**. It is an arkosic sandstone of fluvial origin of 600m to 700m thick **[25]**. Bouity**[26]** distinguishes three lithofacies: the conglomeratic sandstone facies, the coarse and medium quartzo-feldspathic massive sandstone facies and the fine micaceous sandstone facies. The mineralogical composition of these lithofacies is summarized in Table 1. According to Chevalier et al. **[27]**, the heavy minerals in Inkisi sandstone are represented by zircon, tourmaline, apatite, rutile, green beryl and exceptionally corundum. In this profile, the Cover Formation overlies the Inkisi sandstones through an alluvial stone line which itself overlies an Ordovician unconformitypaleosurface**[3]**.

***Table 1**. Mineralogical composition of Inkisi sandstone facies (from Bouity,**[26],** improved by Miyouna (this work)).*

Facies	Quartz (%)	Microcline (%)	Orthose (%)	Plagioclase (%)	Biotite (%)	Muscovite (%)	Debris of Rock (%)	Tourmaline / zircon (%)
Micaceous	63,86	6,71	0,08	4,4	18,52	6,25	0	0,18
Massif	60,15	21,12	0,98	7.83	3	5,2	1,63	0,09
Conglome-ratic	62,17	31,36	1,82	0,56	0	0,04	4,02	0,03

The Profile of "Main bleue" is located in the Stanley-Pool basin. The Stanley-Pool Series currently known as the Stanleyville Group is part of the Congo Supergroup**[1]**. It occurs in D.R. Congo, Angola and Congo (Brazzaville). It is a continental sedimentary Formation, which outcrops around Brazzaville where it is well known, widely visible and discordant on the Inkisi sandstones **[28]; [29]**. It is a fluvio-lacustrine series **[30]** of Jurassic age in its lower part and Cretaceous in its upper part **[24]**. The Stanley-Pool Series is subdivided into three levels **[30]**. The lower level (SP1), known by sampling at the port of Kinshasa and in the Makélékélé ravine, has red argillites with abundant sandstone flowing upwards, superimposed on more or less sandy marls of similar hue. These argillites are silty and stratified. This level is dated to the Upper Jurassic **[31]**, thanks to fossils of ostracods, phyllopods and fish fragments. The middle level (SP2), at least 20 m thick **[30]**, consists of locally indurated white compact sandstones with large cross stratifications. This level is rich in feldspar and is silicified in its upper part, forming the silicified slabs **[17]; [30]**. Finally, the upper level (SP3), about 90 m thick**[32]**, is formed by very soft, kaolinite-rich, silty white sandstone with cross stratifications. The Stanley-Pool Series is surmounted locally by the silicified aeolian sands of the Tékés Plateau Series or by the Cover Formation.

In the profile of the "Main Bleue", the upper part of the Stanley-Pool (SP3) and the Tékés Series are completely gullied. The Cover Formation is underlain by the sands of SP2 through a palaeosurface marked by a complex stone line **[3]**.

2.2 Methodology used

The methodology consisted of the field and laboratory study. The field study consisted in identifying and describing the Cover Formation and its bedrock and sampling. 22 samples were collected for laboratory studies. In the laboratory, the study consisted of extraction, description, identification and heavy mineral counting, analysis and interpretation of results. As heavy minerals are generally concentrated in the 160 µm to 350 µm fraction **[33]**, we chose to extract them in the 125 µm to 250 µm fraction by density using bromoform and the protocol of Parffenoff*and al.***[34]**. The grains of heavy minerals were treated with 50% diluted HCl and 2N oxalic acid to remove carbonate and ferruginous coatings on the grainsfor their better description under polarizing microscope and binocular loupe. Extraction processes and thin-sheet fixation were carried out at the sedimentology laboratory of the "Centre de RecherchesGéologiques et Minières (CRGM)"of Kinshasa, D.R. Congo. The description,

determination and counting of heavy minerals were done under the polarizing microscope and binocular magnifying glass at the Geosciences laboratory of the Faculty of Sciences and Techniques of Marien NGOUABI University of Brazzaville, based on the Atlas of Brochet*et al.*[35] and Devismes[36]. The quantification of heavy minerals was done by counting all the identified minerals crossing the reticule wires on a line crossing the thin blade, by sweeping it completely. The percentage of each mineral was calculated as follows:

$$X = \frac{n}{N \times 100} \qquad \textit{(Equation 1)}$$

wheren = the number of counted points of a heavy mineral;

N = the total number of counted points of all heavy minerals in the entire thin blade.

The results of the counting allowed the statistical treatment by Principal Component Analysis (PCA) in order to understand the relationships existing between the different heavy mineral species, to identify the mineral parageneses characteristic of the Cover Formation and its bedrock as well as the potential sources of these heavy minerals.

III. Results

3.1 Field Study

The profile of Diosso (**Figure 2a**) shows from bottom to top three lithological sets: the lower set representing the "Série des Cirques", the middle set representing the Stone line and the upper set representing the Cover Formation. The "Série des Cirques" of Diosso consists of five (5) lithological units. Unit I consists of a stack of onlap elemental sequences composed of fine and medium sand topped by very fine sand clay or silty clay. The unit ends in a palaeosol. Units II to V are each made up of a stack of onlap elementary sequences generally starting by a gravelly or conglomerate sand, containing large cross stratifications. Each unit begins with a gullying surface bearing a conglomerate or conglomerate sand with cross and parallel plane stratifications and ends with a palaeosol developed on a fine clayey sand or silty clay.

The middle set is a laterite of 0.40 m to 0.90 m of thickness, heavily armoured in its upper part. It is composed of ferruginous pisolites, round and shiny quartz grains, quartzite pebbles, magmatic and metamorphic rocks. The upper set of 12 m thickness constitutes the Cover Formation. It is a yellow ochre,thin sands with a homogeneous appearance.

The profile of the "Pont du Djoué"cliff **(Figure 2b)** shows three sets. The lower set, of about 3.47 m thick is the Inkisisandstone. It is a succession of lenticular elementary sequences of at least 1 m thick. Each lens begins with an erosive surface bearing flattened pebbles of quartzite, magmatic and metamorphic rocks, silexite, carbonate, oolite and red argillite. Above, from bottom to top, appear coarse wine-redconglomeratic sandstones with large cross stratifications, medium wine-red sandstones with small oblique and herringbone stratifications, and fine micaceous and clayey, wine-red sandstones in 5-10 cm platelets and with current ripples marks.

The middle set, from 3.47 m to 5.02 m, represents the alluvial stone line with a thickness varying from 0.60 m to 1.5 m. It is a polygenic, coarsening conglomerate composed of angular and sub-rounded blocks of multi-centimetric size of the silicified slab and laterite, rounded pebbles of Inkisi sandstone, chert, whitish and flattened pebbles of quartzites, magmatic and metamorphic rocks, granules of indurated laterite with ferruginous cement. That stone line contains worn archaeological tools in its middle part and unworn archaeological tools in its upper part. The upper set (5.02 m to 11 m) represents the Cover Formation. It is an ochre-yellow, fine, silty, clayey sand with no sedimentary structures and a homogeneous appearance.

The profile of the "Main Bleue" is located in Bacongodistrict, on the right bank of the Congo River, not far from the De Gaule hut. The outcrop is a cliff more than 40 m high (**Figure 2c**) which shows three sets representing from bottom to top: the Stanley-Pool Series, the Stone line and the Cover Formation. The lower set of 25.30m thick, shows three units: Unit I **(**0 m - 17 m) is composed of 14 m

of medium to fine clayey, whitish-grey sands with cross stratificationsand parallel planes stratificationsshowing alternating beds of fine and medium sand. There are erosion gutters of 10 cm to 15 cm deep and about 1.20 m wide, filled with fine and medium sand showing plane parallel stratifications; 0.5 m of greyish sandy claywith small shrinkage crack at the top, and debris of organic matter. Finally, 3.5 m of silicified slab, consisting of a very fine, much silicified, whitish-grey sandstone with lenticular bedding, locally brecciated beds, containing discontinuous laminae of chalcedony. This slab is strongly silicified, giving in some places a millstone appearance. Unit II (from 17 m to 24.5 m) consists of greyish silty clay with lenticular beddingdrawing festoon cross bedding structures. It contains shrinkage crack in its upper part. It is lightly silicified and also contains discontinuous, whitish, interlayered laminates of chalcedony. This clay is surmounted by 5.50 m of fine to medium, whitish sands with large curved stratifications tangential to the plane parallel stratifications. The plane-parallel stratifications are made up of alternating beds of fine clayey sands with beds of medium to coarse sands. This level contains several erosion gutters, micro faults, slumps and small hydraulic ripples marks. The unit ends with 1 m of very fine, highly silicified clayey sandstone constituting the second slab. Unit III is strongly gullied and is in shreds of about 0.80 m. These are fine to medium, whitish and kaolinic sandstones containing cross stratifications.

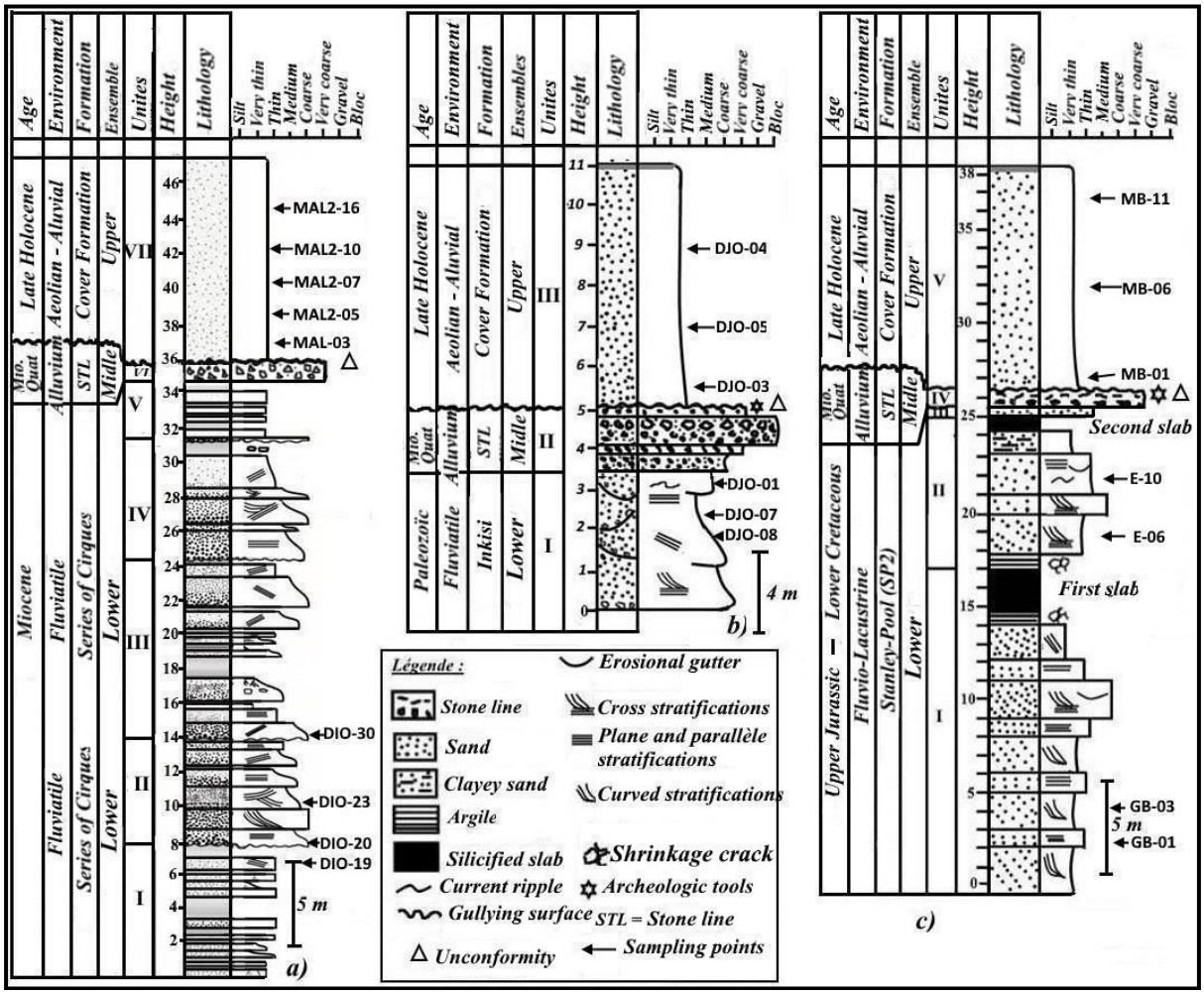

***Figure 2**. Lithostratigraphic log: **a)** Profile of Diosso; **b)** Profile of the "Pont du Djoué"cliff; **c)** Profile of "Main bleue"*

The middle set (from 25.30 m to 26.10 m) represents the stone line. It is a polygenic conglomerate with a sandy-clay matrix, its thickness varying between 0.20 m and 1.20 m. This conglomerate is composed of two levels: the lower level of about 0.20 m thick is composed of rounded and flattened pebbles of quartzite, magmatic and metamorphic rocks, Inkisi sandstone, angular and sub-rounded blocks of the silicified slab, all wrapped in a greyish sandy-clay matrix. The upper level, about 0.50 m

thick, is mainly composed of angular gravels and granules of pisolitic laterite. The sorting is poor and the elements are packed in a red ochre sandy-clay matrix. The upper set (26.10 m - 38.4 m) consists mainly of fine and very fine sand, clay-ochre yellowish-silty, homogeneous in appearance. It ends with about 0.20 m of humus soil.

3.2 Laboratory study

3.2.1 Description and identification of heavy minerals

Fifteen minerals species have been identified in the Cover Formation and his bedrock (**Figure 3**).

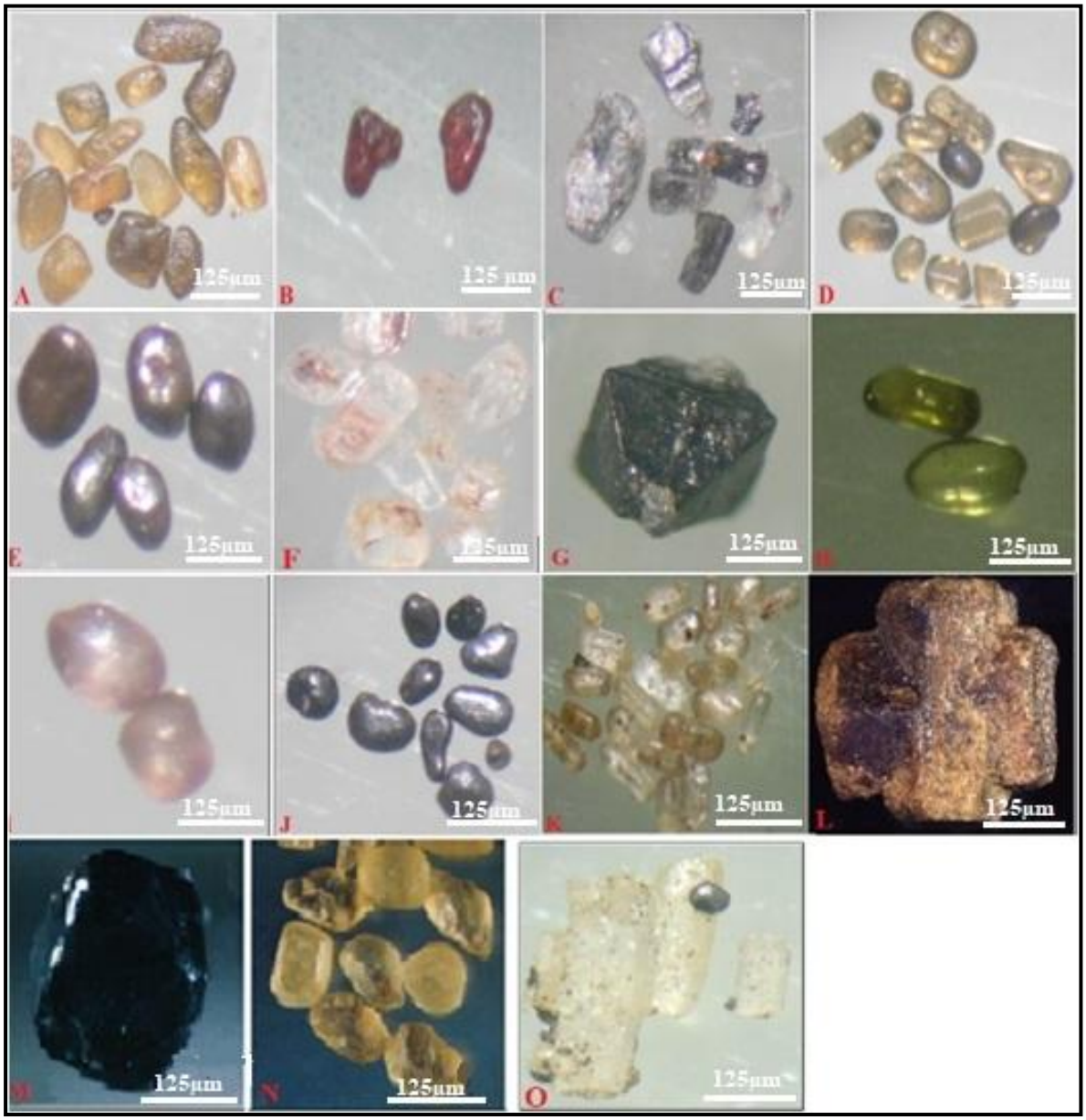

***Figure 3** : Heavy minerals identified in the profiles of Diosso-Malele, "pont du Djoué cliff and "Main bleue": **A**) sphene ; **B**) rutile ; **C**) Kyanite ; **D**) tourmaline ; **E**) limonite ; **F**) sillimanite ; **G**) magnetite ; **H**) amphibole ; **I**) garnet, **J**) ilmenite ; **K**) zircon ; **L**) staurotide ; **M**) spinelle ; **N**) andalousite, **O)** mineral not identified (NI).*

3.2.2. Quantification of heavy minerals

Tables 2, 3 and **4** give the results of the heavy mineral count contained in the selective samples from the profiles of Diosso and Malele, "Pont du Djoué cliff and the Blue Main.

Table 2. *Mineralogical composition of the Cover Formation and its bedrock represented by the Série des Cirques of Diosso*

Formation	Samples	Counting	Tourmaline	Zircon	Garnet	Rutile	Sphene	Staurotide	Kyanite	Sillimanite	Amphibole	Spinelle	Ilmenite	Magnetite	Limonite	Mineral N.I.	TOTAL
Cover Formation	MAL2-16	Number	118	28	0	8	120	0	20	125	34	0	122	0	44	0	619
		%	19,06	4,52	0,00	1,29	19,39	0,00	3,23	20,19	5,49	0,00	19,71	0,00	7,11	0,00	
	MAL2-10	Number	59	7	0	5	48	0	22	100	28	0	71	0	11	0	351
		%	16,81	1,99	0,00	1,42	13,68	0,00	6,27	28,49	7,98	0,00	20,23	0,00	3,13	0,00	
	MAL2-07	Number	119	16	4	20	59	0	34	137	22	0	130	0	3	0	544
		%	21,88	2,94	0,74	3,68	10,85	0,00	6,25	25,18	4,04	0,00	23,90	0,00	0,55	0,00	
	MAL2-05	Number	42	8	0	7	115	0	22	48	38	0	115	0	12	0	407
		%	10,32	1,97	0,00	1,72	28,26	0,00	5,41	11,79	9,34	0,00	28,26	0,00	2,95	0,00	
	MAl2-03	Number	138	37	1	15	115	0	24	326	47	1	250	0	50	0	1004
		%	13,75	3,69	0,10	1,49	11,45	0,00	2,39	32,47	4,68	0,10	24,90	0,00	4,98	0,00	
"Serie des Cirques"	DIO-30	Number	99	103	13	12	364	1	65	705	59	2	1145	2	39	4	2613
		%	3,79	3,94	0,50	0,46	13,93	0,04	2,49	26,98	2,26	0,08	43,82	0,08	1,49	0,15	
	DIO-23	Number	106	30	0	0	246	0	7	71	75	0	295	0	74	2	906
		%	11,70	3,31	0,00	0,00	27,15	0,00	0,77	7,84	8,28	0,00	32,56	0,00	8,17	0,22	
	DIO-20	Number	37	12	3	2	155	0	9	25	28	1	285	0	9	2	568
		%	6,51	2,11	0,53	0,35	27,29	0,00	1,58	4,40	4,93	0,18	50,18	0,00	1,58	0,35	
	DIO-19	Number	40	11	0	1	51	0	20	129	17	4	175	0	8	1	457
		%	8,75	2,41	0,00	0,22	11,16	0,00	4,38	28,23	3,72	0,88	38,29	0,00	1,75	0,22	

Table 3. *Mineralogical composition of the Cover Formation and its bedrock represented by the Inkisi sandstones in the profile of the "Pont du Djoué" cliff*

Formation	Samples	Depth (m)	Counting	Tourmaline	Zircon	Rutile	Anatase	Sphene	Staurotide	Kyanite	Garnet	Sillimanite	Amphibole	Ilmenite	Limonite	TOTAL
Cover Formation	**DJO-04**	**9**	Number	132	15	18	0	120	0	20	0	96	5	122	44	572
			%	23,08	2,62	3,15	0,00	20,98	0,00	3,50	0,00	16,78	0,87	21,33	7,69	
	DJO-05	7	Number	150	5	23	0	81	7	12	1	45	3	97	37	461
			%	32,54	1,08	4,99	0,00	17,57	1,52	2,60	0,22	9,76	0,65	21,04	8,03	
	DJO-03	**5**	Number	59	7	16	0	48	4	22	0	37	6	56	11	266
			%	22,18	2,63	6,02	0,00	18,05	1,50	8,27	0,00	13,91	2,26	21,05	4,14	
Inkisi	**DJO-01**	**3**	Number	62	4	7	10	0	0	1	2	0	0	52	20	158
			%	39,24	2,53	4,43	6,33	0,00	0,00	0,63	1,27	0,00	0,00	32,91	12,66	
	DJO-07	**2,3**	Number	68	2	5	14	0	0	3	2	0	0	49	23	166
			%	40,96	1,20	3,01	8,43	0,00	0,00	1,81	1,20	0,00	0,00	29,52	13,86	
	DJO-08	**1,95**	Number	94	3	9	23	0	0	1	1	0	0	50	16	197
			%	47,72	1,52	4,57	11,68	0,00	0,00	0,51	0,51	0,00	0,00	25,38	8,12	

Table 4. *Mineralogical composition of the Cover Formation and its bedrock represented by the Stanley-Pool in the "Main Bleue" profile*

Formation	Samples	Counting	Tourmaline	Zircon	Rutile	Anatase	Sphene	Staurotide	Kyanite	Garnet	Sillimanite	Amphibole	Spinelle	ilmenite	Magnetite	Limonite	TOTAL
Cover Formation	MB-11	Number	150	5	23	0	77	12	4	2	45	3	0	210	0	47	501
		%	29,94	1,00	4,59	0,00	15,37	2,40	0,80	0,40	8,98	0,60	0,00	41,92	0,00	9,38	
	MB-06	Number	162	7	4	0	53	13	9	0	40	2	0	182	0	32	451
		%	35,92	1,55	0,89	0,00	11,75	2,88	2,00	0,00	8,87	0,44	0,00	40,35	0,00	7,10	
	MB-01	Number	65	2	2	0	62	9	2	1	9	2	0	120	0	14	226
		%	28,76	0,88	0,88	0,00	27,43	3,98	0,88	0,44	3,98	0,88	0,00	53,10	0,00	6,19	
Stanley-Pool	E-06	Number	49	1	5	0	0	3	0	0	0	0	0	40	0	13	111
		%	44,14	0,90	4,50	0,00	0,00	2,70	0,00	0,00	0,00	0,00	0,00	36,04	0,00	11,71	
	E-10	Number	40	2	4	0	0	0	1	1	0	0	0	80	0	32	160
		%	25,00	1,25	2,50		0,00	0,00	0,63	0,63	0,00	0,00	0,00	50,00	0,00	20,00	
	GB-03	Number	51	2	5	0	0	3	1	0	0	0	0	39	0	14	115
		%	44,35	1,74	4,35	0,00	0,00	2,61	0,87	0,00	0,00	0,00	0,00	33,91	0,00	12,17	
	GB-01	Number	35	3	3	0	0	2	2	1	0	0	3	23	0	15	87
		%	40,23	3,45	3,45	0,00	0,00	2,30	2,30	1,15	0,00	0,00	3,45	26,44	0,00	17,24	

These tables show that heavy minerals are less abundant in the Cover Formation (0.01 to 0.2% of the initial sample mass) than in its bedrock (0.2 to 0.8%). These heavy minerals are dominated by ubiquitous minerals, mainly ilmenite, tourmaline, zircon, rutile, followed by metamorphism minerals such as sillimanite, kyanite, andalusite, garnet and staurotide; magmatism minerals such as spinel, sphene and other common minerals such as magnetite, green amphibole, limonite.

In the Diosso profile (**Figure 4a**)the ilmenite is the most abundant heavy mineral, followed by sillimanite and sphene. This is followed by tourmaline, zircon, green amphibole, limonite, rutile, and garnet. These heavy minerals are rounded except for spinel, sillimanite, staurotide and kyanite, which are sub angular and even prismatic. In the Cover Formation, ilmenite, sillimanite, sphene, and tourmaline are the most abundant heavy minerals. Next come amphiboles, kyanite, zircon, and limonite. Garnet and rutile are scarce. The kyanite, sillimanite, staurotide are sub rounded. Tourmaline and zircon are much worn, while others are still prismatic. Several grains of the heavy minerals of the Cover Formation bear impact marks unlike those of the "Série des Cirques" of Diosso. Red hematite, although very abundant compared to all other minerals, was not considered in the statistical study. Its angular shape and leaf habit show that it results from current pedogenetic processes. The "Série des Cirques" of Diosso is characterized by the following heavy mineral paragenesis: ilmenite, sillimanite, sphene, tourmaline, amphibole and zircon, while the Cover Formation is characterized by the ilmenite, sillimanite, sphene and tourmaline paragenesis (**Figure 4a**).

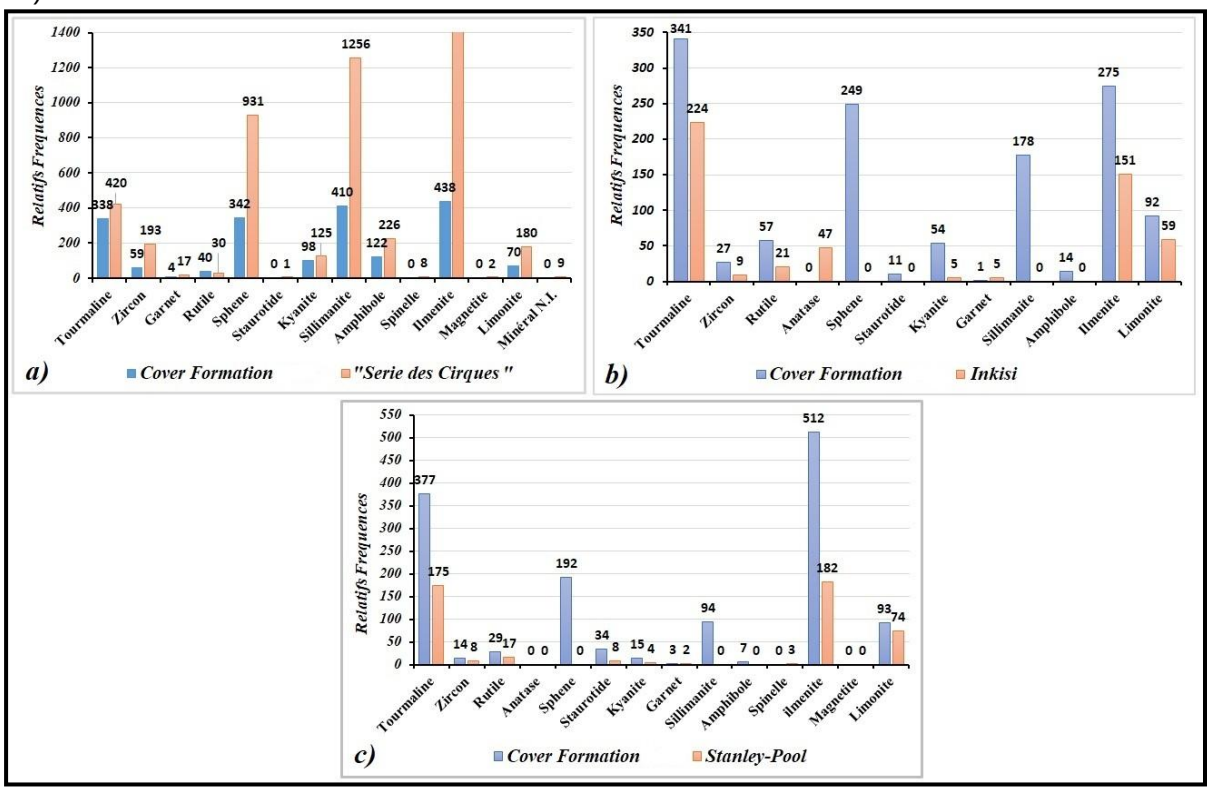

Figure 4. *Relative frequencies of heavy minerals in the Malele Cover Formation and its bedrock:* ***(a)****Diosso and Malele profile,* ***(b)****"Pont du Djoué cliff profile,* ***(c)****Main bleue profile*

In the profile of the "Pont du Djoué" cliff (**Figure 4b*)***, the heavy minerals identified in the Inkisi sandstones are, in order of decreasing abundance: tourmaline, ilmenite, limonite, anatase, rutile, zircon, kyanite, garnet. These minerals are sub angular. Those identified in the Cover Formation are, in decreasing order of abundance: tourmaline, ilmenite, sphene, sillimanite, limonite, rutile, kyanite, zircon, green amphibole, staurotide. Contrary to those described in the Inkisi sandstones, those of the Cover Formation bear shot marks similar to those observed on the heavy minerals of the Malele Cover Formation. Sillimanite and kyanite are either prismatic or sub-rounded. Tourmaline and zircon are much worn out, while others are prismatic or even automorphic. The dominant heavy mineral paragenesis in the Cover Formation is composed of tourmaline, ilmenite, sphene and sillimanite,

while that of the Inkisi sandstones is composed of tourmaline, ilmenite, limonite and anatase. Anatase is absent in the Cover Formation, whereas sphene, staurotide, sillimanite and green amphibole are absent in the Inkisi sandstones (**Figure 4b**).

In the profile of "Main bleue" (**Figure 4c**), the heavy minerals identified in the Staley-Pool are, in decreasing order of abundance: ilmenite, tourmaline, rutile, zircon, staurotide, kyanite, kyanite, garnet, spinel. These minerals are much worn out, some grains are rounded.

In the Cover Formation, the heavy minerals identified are the following, in decreasing order of abundance: ilmenite, tourmaline, sphene, sillimanite, limonite, rutile, staurotite, zircon, kyanite, amphibole, garnet. These heavy minerals are angular, broken and bear fresh choc marks. Some zircons and tourmalines are prismatic. The dominant heavy mineral paragenesis in the Stanley-Pool is in decreasing order of abundance: ilmenite, tourmaline, limonite and rutile. The dominant heavy mineral paragenesis in the Cover Formation consists of ilmenite, tourmaline, sphene, sillimanite and limonite. Sillimanite, sphene and amphiboles, present in the Cover Formation, are absent in the Stanley-Pool Series, while spinel and anatase are absent in the Cover Formation. The Cover Formation differs qualitatively and quantitatively from its bedrock represented by the Stanley-Pool.

3.3. Principal Component Analysis (PCA)

3.3.1. Profile of Diosso-Malélé

Principal component analysis shows that the factorial planes (F1, F2) and (F1, F3) account for 78.15% and 73.36% of the total variability of the observation points or variables, respectively. The first two planes represent the variability contained in the data set. The study of the cloud of variables in the (F1, F2) plane (**Figure5a**) reveals mineral parageneses grouped into two clouds: the first cloud relating to the F1 axis is made up of sillimanite, ilmenite, magnetite, zircon, sphene, garnet, rutile, staurotide and the second relating to the F2 axis is made up of tourmaline, amphibole and limonite. Spinel and rutile seem to deviate from these two clouds.

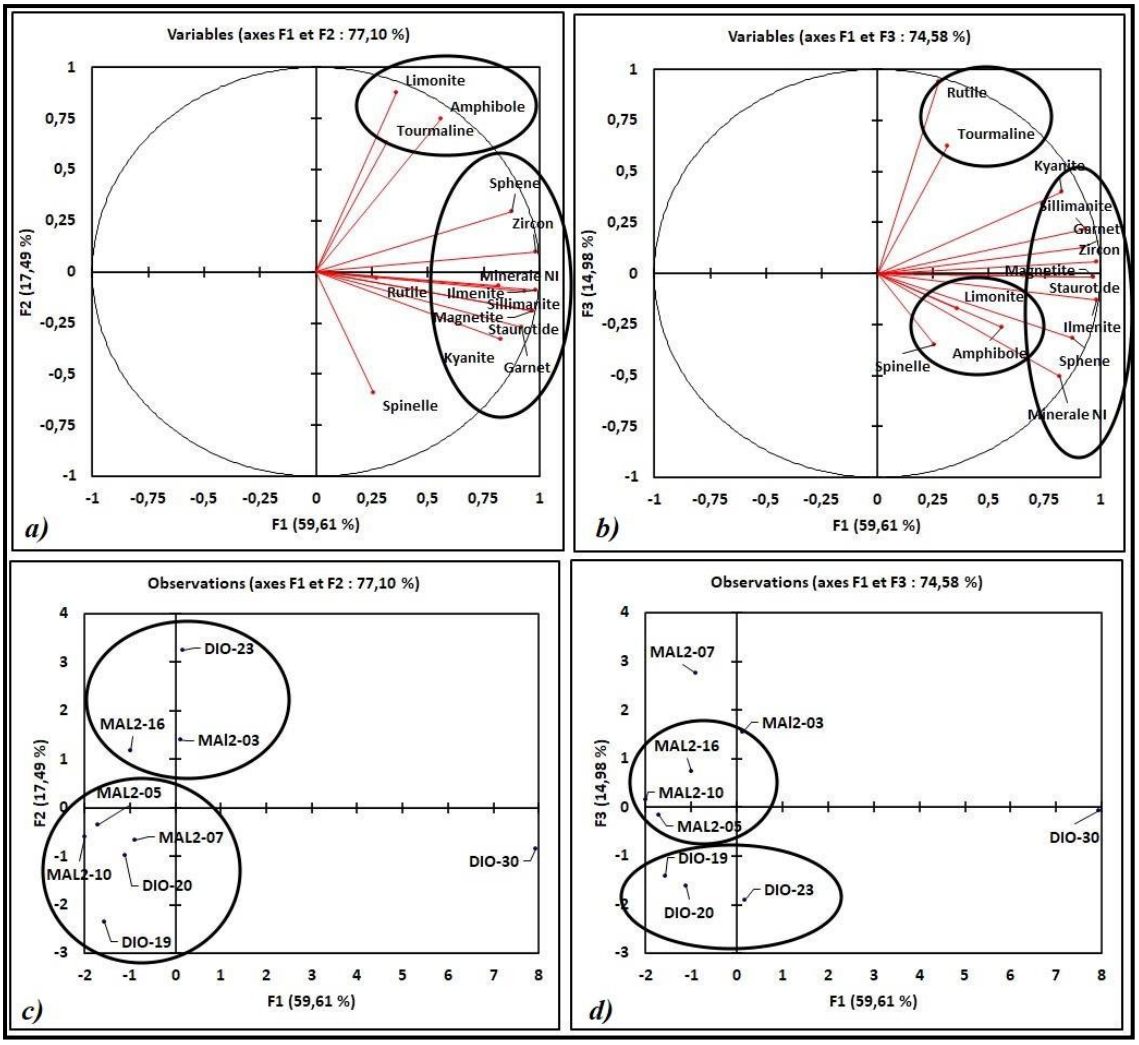

Figure 5*.Cloud of mineral and samples in the (F1, F2) and (F1, F3) planes of the Diosso series of Cirques (DIO-19, DIO-20, DIO-23, DIO-30) and the Malélé Cover Formation (MAL2-03, MAL2-05, MAL2-07, MAL2-10, MAL2-16)*

The plane (F1 and F3) **(Figure 5b)** shows mineral parageneses grouped into three clouds: the first and second clouds refer to the F1 axis and the third to the F3 axis. The first cloud is composed of kyanite, zircon, staurotide, magnetite, garnet, ilmenite; the second cloud by amphibole, limonite and spinel, and the third by tourmaline and rutile.

The study of the observation point cloud (the samples) shows two opposing sample clouds in the plane (F1, F2) (**Figure5c**). The first cloud that is negatively correlated with respect to F1 is composed of samples MAL2-05, MAL2-10, MAL2-07, DIO-20 and DIO-19. This first cloud is strongly opposed to sample DIO-30. The second cloud which is positively correlated with respect to F2 is composed of MAL2-16, MAL2-03 and DIO-23. It negatively opposes the first cloud with respect to F2. The (F1, F3) plane (**Figure5d)** shows two sample clouds that stand out clearly and discriminate well between the "Series des Cirques" and the Cover Formation samples. The first cloud relating to the F1 axis consists of samples MAL2-10, MAL2-05, MAL2-16. The second cloud relating to F3 consists of the samples DIO-19, DIO-20 and DIO-23. In this plane, samples MAL2-07 and MAL2-03 strongly oppose the second cloud.

3.3.2. Profile of "Pont du Djoué"Cliff

Principal component analysis shows that the factorial planes (F1, F2) and (F1, F3) account for 95.71% of the total variability of the cloud of observation points or variables. The first two planes represent very well the variability contained in the data set. In the (F1, F2) plane (**Figure6a)**, the

heavy mineral clouds show four clouds: the first relating to the F1 axis is composed of zircon, sphene, rutile and sillimanite. The second referring to axes F1 and F2 is composed of tourmaline, ilmenite and limonite. The third, relating to axes F1 and F2, is composed of staurotide, kyanite and amphibole, and the fourth, which opposes the third, is composed of garnet and anatase.

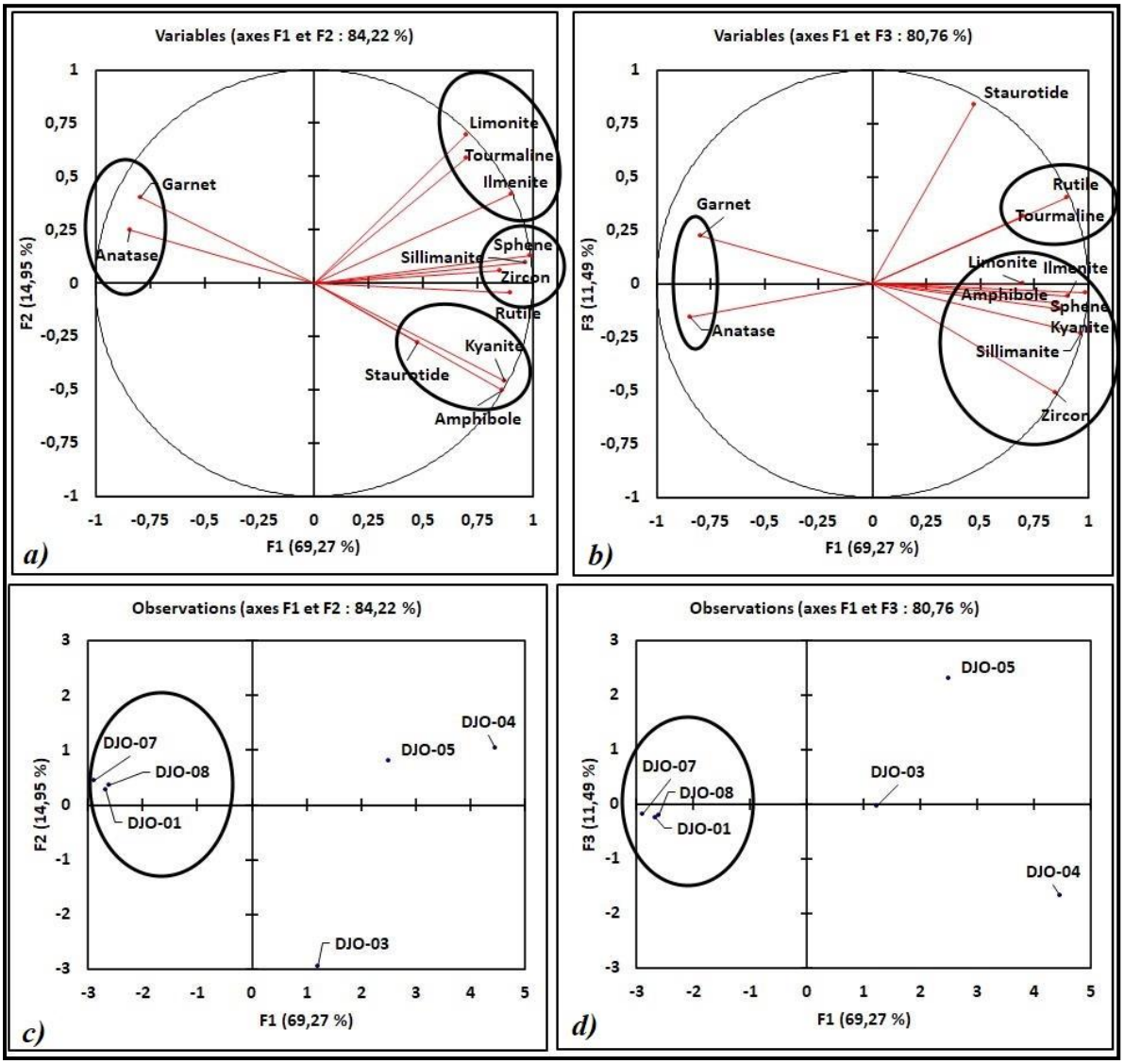

Figure 6*. Clouds of heavy minerals and samples in planes (F1, F2) and (F1, F3) in the Inkisi sandstones (DJO-01, DJO-07, DJO-08) and the Cover Formation (DJO-03, DJO-04, DJO-05) outcropping in the cliff of the "Pont du Djoué".*

The plane (F1, F3) shows three heavy mineral clouds (**Figure 6b*)***: The first is composed of sillimanite, kyanite, ilmenite, sphene, zircon, limonite and amphibole. The second is composed of tourmaline and rutile and the third is formed by anatase and garnet.

With respect to the samples, the (F1, F2) plane (**Figure 6c*)*** shows a cloud composed of samples DJO-01, DJO-07, DJO-08 of the Inkisi sandstones, negatively correlated with the F1 axis and opposing samples DJO-03, DJO-04, DJO-05 of the Cover Formation. The plane (F1, F3) presents an organization identical to that described above and marked by a cloud containing samples DJO-01, DJO-07, DJO-08 of the Inkisi sandstones, negatively correlated with the F1 axis and which opposes samples DJO-03, DJO-04, DJO-05 of the Cover Formation (**Figure 6d).** Principal component analysis shows a clear mineralogical distinction between the Inkisi sandstone and the Cover Formation.

3.3.3. Profile of the "Main bleue"

The (F1, F2) plane (**Figure 7a**) shows two clouds of points. The first one relating to F1 axis is composed of sillimanite, ilmenite, zircon, sphene, staurotide, kyanite, amphibole and tourmaline.

The second cloud, which refers to F2, is composed of garnet and rutile. The spinel deviates negatively from the first cloud. The (F1, F3) plane (**Figure7b*)*** also shows two clouds of points related to F1 axis. The first cloud consists of tourmaline, sillimanite, staurotide, rutile, sphene, amphibole, ilmenite and limonite. The second consists of garnet, zircon and kyanite. According to this plan, the spinel spreads out and also opposes the two mineral clouds.

With respect to the samples, the (F1, F2) plane (**Figure 7c**) shows a cloud which relates to the F1 axis, consisting of samples GB-01, GB-02, E-06 and E-10 all belonging to the Stanley-Pool, and which opposes samples MB-01, MB-06 and MB-11 of the Cover Formation. The (F1, F3) plane (**Figure 7d**) also shows along the F1 axis, a cloud of the samples (E-06, E-10, GB-03) belonging to the Stanley-Pool which opposes samples MB-06 and MB-11 of the Cover Formation. Principal component analysis shows a clear mineralogical distinction between the Stanley-Pool and Cover Formation samples.

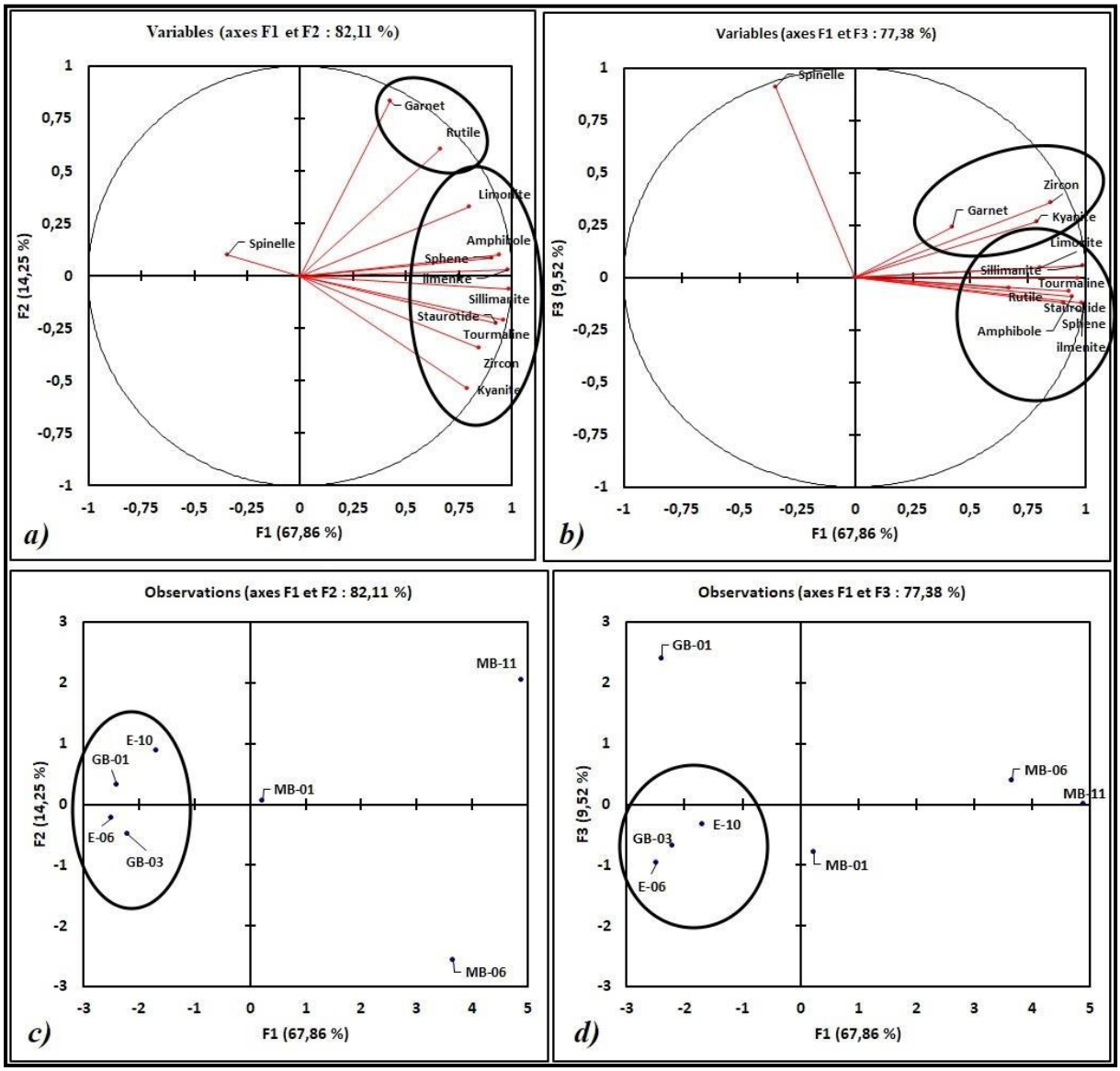

Figure 7*. Clouds of heavy minerals and samples in planes (F1, F2) and (F1, F3), contained in the Stanley-Pool (GB-01, E-06, E-10) and Cover Formation (MB-01, MB-06, MB-11) outcropping in the "Main bleue" profile.*

IV. Interpretation and discussion of results

The field study shows that in all three studied profiles, the Cover Formation overlies its bedrock via a polymictic or polygenic coarsening up orthoconglomerate or via a palaeosol. This coarsening up sorting is indicative of sedimentary dynamics and the increasing of the transport currents competence. These observations confirm those of Thiéblemont **[15]** in Gabon andMiyouna*et al.* (2016, 2019) in Congo, who show that the stone line marks a paléosurface and a gully unconformity. This means that a long time separate the setting up of the Cover Formation of his bedrock.

The study of the heavy minerals of the three studied profiles, shows that heavy minerals are less abundant in the Cover Formation (about 0.01% to 0.3% of the initial sample weight) than in the bedrock (about 0.8% of the initial sample weight). These percentages are identical to those obtained by Le Maréchal **[17]** in the Nganga-Lingoloand Inoni, respectively in Brazzaville and Pool Departments. The heavy minerals identified in the Cover Formation are, in decreasing order of abundance: ilmenite, sillimanite, sphene, tourmaline, amphibole, kyanite, limonite, zircon, rutile and garnet. This list is similar to that obtained by Le Maréchal **[17]** in Congo and by Thiéblemont **[15]** in Gabon, except for the apatite that we did not observe in our samples of the Cover Formation. Figure 4 shows that regardless of the lithological nature of the bedrock, the Cover Formation contains the same paragenesis of heavy minerals, dominated by ilmenite, sillimanite, sphene, tourmaline and zircon. This paragenesis distinguishes it from the bedrock, which contains more diverse and abundant heavy minerals. Regardless of the bedrock, the homogeneity in heavy mineralsof the Cover Formation over long distances from Pointe Noire to Brazzaville, and from Congo Brazzaville to Gabon, regardless of the bedrock, suggests that it does not come from *in-situ*weathering of its basement, contrary to Le Marechal **[17]** and Schwartz **[9]**,**[18]** who believe that the Cover Formation is the product of *in-situ*weathering of its basement. The shot marks on the heavy minerals of the Cover Formation are evidence of their aeolian origin. According to Pojar*et al.***[37]**, it is possible to determine the source or the originof the sediment from the association of heavy minerals containedin a sediment. The angular, sub-rounded sometimes sub-automorphic kyanite, sillimanite, staurotide and green amphibole, associated with garnet, indicate a metamorphic provenance of the green shale and amphibolite facies. Well-rounded tourmaline and zircon show evidence of reworking or recycling of ancient sedimentary or meta-sedimentary rocks. On the other hand, the sub-automorphic zircons and tourmalines associated with rutile undoubtedly suggest magmatic felsicrock origin such as granites, diorites, syenites, granodiorites and associated lavas. Well-worn ilmenite and limonite reveal a long history and several sedimentary cycles. They have been reworked from sediments derived from the alteration of magmatic or metamorphic rocks, rich in ferromagnesian minerals such as diorites, granodiorites, tonalites and their volcanic equivalents. All these characteristics show that the heavy minerals contained in the Cover Formation come from feeding areas that contained mainly metamorphic rocks and secondarily magmatic and sedimentary or meta-sedimentary rocks. Such rocks exist in the Mayombemountain and the Chaillu massif **[23]; [38]**. However, the fact that the Cover Formation retains the same paragenesis of heavy minerals regardless of the geological nature of the bedrock and the fact that these heavy minerals bear shot marks, rule out the hypothesis of *in-situ* alteration of its bedrock and therefore his autochthony. The homogeneity of the paragenesis of the heavy minerals supposes that the sediments of the Cover Formation come from the same distant source.

In the profile of Diosso - Malélé, in the (F1, F2) plane (**Figure5a**), the two clouds formed respectively by the samples (DIO-23 of the "Série des Cirques" and MAL2-16, MAL2-03 of the Cover Formation) (DIO-19, DIO-20 of the "Série des Cirques" and MAL2-05, MAL2-07, MAL2-10 of the Cover Formation) assume that these samples have similar heavy mineral compositions. On the other hand, the (F1, F3) plane (**Figure5b*)*** shows two distinct clouds that discriminate samples DIO-19, DIO-20, DIO-23 of the "Série des Cirques" from samples MAL2-05, MAL2-10, MAL2-16, MAL2-03 and MAL2-07 of the Cover Formation. This shows that from the point of view of heavy mineral content, the sediments of the "Série des Cirques of Diosso and the Malele Cover Formation have similarities and dissimilarities that allow them to be qualitatively and quantitatively distinguished.

In the profile of the "Pont du Djoué" cliff of the heavy minerals identified in the Inkisi sandstones are: tourmaline, rutile, anatase, zircon, ilmenite, limonite, associated with some kyanite, garnet, magnetite and brown hematite. These minerals generally angular, sub-angular and don't bear shot marks, indicating proximity of the area that supply the sediments and a transport agent other than wind. According to Boudzoumou**[25]**, **[1],[26]** the Inkisi sandstones are of fluvial origin. On the other hand, heavy minerals of the Cover Formation, represented by ilmenite, tourmaline, rutile, zircon, associated with sphene, kyanite, sillimanite, staurotide, garnet, limonite, magnetite and brown hematite, which are strongly worn and still bear visible shot marks, show that they were recycled and transported by wind for a long time before being immobilized in a continental environment. In this profile, the Inkisi sandstones and the Cover Formation are easily distinguished qualitatively and quantitatively by their heavy mineral content. Principal component analysis shows that in the (F1, F2), (F1, F3) planes (**Figure6a, 6b*)***,**thedifferent mineral clouds form parageneses point firstly towards metamorphic rocks of green shale grade and amphibolite grade, and secondly towards magmatic rocks. In planes (F1, F2) and (F1, F3) (**Figure6c, 6d)**, the two clouds of samples respectively composed of samples (DJO-01, DJO-07, DJO-08) of the Inkisi sandstones and (DJO-03, DJO-04, DJO-05) of the Cover Formation and which negatively oppose each other with respect to the F1 axis show that the Inkisi sandstones and the Cover Formation have diametrically opposed heavy mineral compositions. This shows that the yellow ochre sands of the Cover Formation overlying the Inkisi sandstones are not the product of *in-situ* weathering of the Inkisi sandstones.

In the "Main bleue" profile, the heavy minerals identified in the Stanley-Pool are ilmenite, tourmaline, rutile, zircon, staurotide, kyanite, garnet, and spinel. The fact that these heavy minerals are well-worn and sometimes bear polished shot marks suggests an aquatic recovery after an aeolian phase. On the other hand, in the Cover Formation the heavy minerals identified are ilmenite, tourmaline, sphene, sillimanite, limonite, rutile, staurotide, zircon, kyanite, amphibole and garnet. These heavy minerals are worn, commonly broken, and bear fresh shot marks indicating that they have been subjected to a final aeolian process before being immobilized. Qualitatively and quantitatively, the Cover Formation differs clearly from the Stanley-Pool by its heavy mineral content.

The two clouds of heavy minerals in the plane (F1, F2) (**Figure7a**) formed respectively by sillimanite, ilmenite, zircon, sphene, staurotide, kyanite, amphibole, limonite and tourmaline for the first and garnet and rutile for the second, point towards metamorphic rocks of the green shale and amphibolite grades. The spinel that deviates negatively from the first cloud indicates an origin from mafic or ultramafic rocks deficient in quartz. In the (F1, F3) plane (**Figure7b**), the two clouds formed respectively of tourmaline, sillimanite, staurotide, rutile, sphene, amphibole, ilmenite and limonite for the first one and zircon, kyanite and garnet for the second one, confirm that the provenance area contains mainly metamorphic and secondarily magmatic rocks.

The distinct clouds (**Figure7c**) formed by the samples (GB-01, GB-03, E-06 and E-10) from the Stanley-Pool and the samples MB-01, MB-06 and MB-11 from the Cover Formation which oppose each other in the (F1, F2), (F1, F3) planes, show that these two formations have mineralogical compositions which clearly distinguish them. In the "Main bleue" profile, the Cover Formation has a much more different mineralogical composition than the Stanley-Pool. It is therefore not the result of theweathering of its bedrock formations represented by the Stanley-Pool.

To sum up, in the three studied profiles, the Cover Formation has the same and homogeneous heavy minerals composition. It is easily distinguished from its bedrock. These heavy minerals, dominated by the ubiquitous, mainly come from the metamorphic rocks of green shale and amphibolite grades, and secondarily, from magmatic and sedimentary rocks. Some of these minerals have undergone several sedimentary recycling processes.

V. Conclusion

The Cover Formation overlies its bedrock of varied lithological nature through a palaeosurfacematerialized by an alluvial or colluvial stone line, polymicte or oligomicte conglomerate. The Cover Formation contains a same and homogeneous paragenesis of heavy minerals dominated by ilmenite, sillimanite, sphene, tourmaline, amphibole, kyanite, limonite, zircon, rutile and garnet,

whatever the geological nature of the bedrock. This paragenesis distinguishes qualitatively and quantitatively the Cover Formation from its bedrock. These heavy minerals found in the Cover Formation originate mainly from the weathering profiles of ancient metamorphic rocks of green shale amphibolites grades, and secondarily, from magmatic rocks with felsic tendency rich in ferromagnesium, and finally from the weathering profiles of ancient sedimentary or metasedimentary rocks. These heavy minerals have undergone several sedimentary recyclings and have been transported by the wind. Itappears clearly, according to the heavy minerals, the Cover Formation does not result from *in-situ*weathering of its bedrock. It comes from a distant source and must therefore be stratigraphically separated from its bedrock as proposed by Thiéblemont et *al*. (2009) in Gabon.

VI. Acknowledgements

We would like to thank all the staff of the sedimentology laboratory of the "Centre de RecherchesGéologiques et Minières"of Kinshasa (RDC) for the quality of the extractions and treatments carried out on the heavy minerals, which undoubtedly facilitated their determination. We would like to thank the General Manager of Congo Exploration who provided us with the necessary means during the field study. We thank MrJoachim MIYOUNA for the English translation. We also thank the anonymous reviewer for the quality of the observations and suggestions that improved the quality of this manuscript.

References

[1] **Callec, Y., Beaur H., Paquet F., Prognon F., Issautier B., Schoetter J-M., Thiéblemont D., Boudzoumou F., Guillochau F., KebiTsoumou S., Dah Tolingbonon R. H., NgangaLumuamu F. (2015a)**. Notice explicative de la carte géologique de la République du Congo à 1/100 000, Feuille Brazzaville. *Editions BRGM*. 129 p.

[2] **Miyouna, T., Malounguila-Nganga, D.M., Essouli, O.F., Ndembé-Nbembé, A. J., Moussiessié, J., Kinga-Mouzéo, Boudzoumou, F. (2016)**. Etude Paléoenvironnementale des dépôts détritiques de la Formation de couverture du bassin côtier du Congo. *Rev. CAMES*, Vol. 04, n°01, ISSBN : 2424 – 7235, 35 – 44.

[3] **Miyouna, T., Elenga, H., Boudzoumou, F., Essouli, O. F., IbaraGnianga, A., Sow, E. H. (2019**). Dynamique sédimentaire de la Formation de couverture de Pointe Noire à Brazzaville, sud de la République du Congo. *Afrique Science*, 15 (4), ISSN 1813-548X, 134 – 155.

[4] **Vincent, P.L. (1965)**. Les formations meubles superficielles au sud du Congo et du Gabon. Mission 1964 – 1965. *Rapport BRGM*, 65 BRA 009.

[5] **Vogt, J., Vincent, P.L. (1966)**. Terrains d'altération et de recouvrement en zone intertropicale. *Bull. BRGM*, 4, 1–111.

[6] **Dadet, P. (1969)**. Notice explicative de la carte géologique de la République du Congo Brazzaville au 1/500 000. Mem. *Bur. Rech. Geol. Min*. Orléans, France 70, 103p.

[7] **Sitou, L., Tchicaya, J. (1991)**. L'érosion en cirques dans la région côtière du Congo. *Bulletin de la Société Géographique de Liège*. 27, 77-91, 13p.

[8] **Schwartz, D. (1992)**. Assèchement climatique vers 3000 B.P. et expansion Bantu en Afrique centrale atlantique : quelques réflexions. *Bull. Soc. Géol. France*, 163 (3), pp 353–361.

[9] **Schwartz, D. (1996**). Archéologie préhistorique et processus de formation des stone lines en Afrique centrale (Congo-Brazzaville et zones périphériques). Seminar on Géo-archeology*In*: Tropical and Mediterranean Regions, Brussels, April 1996. Royal Academy of Overseas, Sciences. *Geo-Eco-Trop*, 20 (1-4), 15–38.

[10] **Mercader, J., Marti, R., Martinez, J. L., Brooks, A. (2002)**. The nature of the stone lines in the African Quaternary Record: archaeological resolution at the rainforest site of Mosumu, Equatorial Guinea. *Quaternary International*, 89, 71-96.

[11] **Lecomte, P. (1988)**. Stone line profiles: Importance in geochemical exploration. *Journal of Geochemical Exploration*, 30, 35-61.

[12] Rünge, J. (2001). On the age of stone-lines and hillwash sediments in the eastern Congo basin –palaeoenvironmental implications. *In*: Heine K. (Ed.), Palaeocology of Africa and the surroundings islands. Proc. XVth*INQUA Conference*, pp. 19-36.

[13] Alexander, J. (2002). Les cuirasses latéritiques et autres formations ferrugineuses tropicales : Example du haut Katanga méridional. Musée Royal Afrique centrale, Tevuren. *Ann Sc. Géol.*,107, 2002.

[14] Thiéblemont, D., Castaing, C., Billa, M., Bouton, P., Préat, A. (2009). Notice explicative de la carte géologique et des ressources minérales de la République Gabonaise à 1/1.000.000. 3e édition, *BRGM*, n°249, 260-261p.

[15] Thiéblemont, D. (2013). Evidence for an aeolian origin of the Holocene lateritic surface cover of Gabon. *Quat. Int*. 296, 176–197.

[16] Cauxeiro, C. (2013). Architecture stratigraphique du prisme néogène de La Cuanza, Angola et relations avec les mouvements verticaux. Ph. D. Univ. Montpelier 2, 307 p.

[17] Le Maréchal, A. (1966). Contribution à l'étude des plateaux Batéké (Géologie, géomorphologie, hydrogéologie). Office de la Recherche Scientifique et Technique Outre-Mer, Centre de Brazzaville, Service géologique, Rapport, 78 p.

[18] Schwartz, D. (2014). Comment on: Geochronological arguments for a close relationship between surficial formation profiles and environmental crisis (C. 3000 – 2000 B.P.) in Gabon (Central Africa) – D. Thieblemont*et al*., 2013, *C.R. Geoscience*, 345, 272-283.

[19] Brownfield, M.E., and Charpentier, R.R. (2006). Geology and total petroleum systems of the West Central Coastal Province (7203), West Africa: *U.S. Geological Survey Bulletin* 2207-B, 52p.

[20] Frimel, H. E., Tack, L., Basei, M. S., Nutman, A. P., Boven, A. (2006). Provenance and chemostratigraphy of the Neoproterozoïc West congolian Group in the Democratic Republic of Congo. *Journal of African Earth Sciences*, 46, 221 – 239.

[21] Straathof, G.B. (2011). Neoproterozoic Low Latitude Glaciations: An African Perspective. Unpublished PhD *Thesis*, University of Edinburgh, 285p.

[22] Cahen, L. (1983). Le Groupe du Stanleyville (Jurassique supérieur et Wealdien de l'intérieur de la République du Zaïre) : Révision des connaissances. Rapport annuel du Musée Royal de l'Afrique centrale, Tervuren (Belgique), Département de Géologie et de la Minéralogie, p. 73 – 91.

[23] Desthieux, F., Boudzoumou, F., Mompossa, F., Akiaoue, E., Missamou, A., Malera, M., Kiba, V. (1993). Carte géologique de la République du Congo à 1/100.000. Ministère des Mines et de l'Energie.

[24] Callec, Y., Lasseur, E., Le Bayon, B., Thiéblemont D., Fullgraf, T., Gouin, J., Paquet F., Le Metour, D. J., Delhaye-Brat, V., Giresse, P., Malounguila-Nganga, D. M., Boudzoumou F. (2015b). Notice explicative de la carte géologique de la République du Congo à 1/200 000, Feuille Pointe Noire. *Editions BRGM*. 213 p.

[25] Boudzoumou, F. (1986). La chaine Ouest-Congolienne et son avant- pays au Congo : Relation avec le Mayombien, Sédimentologie des séquences d'âge protérozoïque supérieur. *Thèse de doctorat 3e cycle*. Université d'Aix- Marseille III, 216p.

[26] Bouity, L. (2016). Caractérisation sédimentologique et géotechnique des différents faciès des grès de l'Inkisi. *Mémoire de master*, Faculté des Sciences et Techniques Université Marien NGouabi. 52p.

[27] Chevalier, D., Giresse, P., Massengo, A., Botokou, G. (1972). Le site de Brazzaville ou contribution à une notice explicative de la carte géologique de Brazzaville. *Annale Université Brazzaville*, 8, 17 – 42.

[28] Giresse, P. (1982). La succession des sédimentations dans les bassins marins et continentaux du Congo depuis le début du Mésozoïque. *Sci. Geol. Bull*. 35 (4), 183 – 206.

[29] Mouyoungou, J. (1990). Les silicifications mésozoïques et cénozoïques de la bordure occidentale du Bassin de Paris et de la région de Brazzaville au Congo. *Thèse 3e cycle*, Université d'Angers. UFR Sciences de l'environnement. 242p.

[30] Giresse, P. (1990). Paleoclimatic and structural environment at the end of the Cretaceous along the Western flank of the congo Basin, with application of underground microdiamonds around Brazzaville. *Journal of African Earth* Sciences 10: 399 – 408.

[31] Nicolini, P., et Roger, J. (1951). Sur la présence des fossiles dans le Karroo à Brazzaville (Congo). *Comptes Rendus Académie des Sciences*, Paris 223, 1127 – 1129.

[32] Mestraud, J-L. (1964). Carte géologique de la République centrafricaine au 1/1500000. BRGM, Paris.

[34] Parffenoff, A., Pomerol, C., Tourenq, J. (1970). Les minéraux en grain, Méthodes d'étude et détermination. *Masson, et Cie Paris VI*, 550 p.

[35] Broche, J., Casanova, R., Loup, G. (1977). Atlas des minéraux en grains, identification par photographie en couleur. Société pour le développement Minier de la Côte d'Ivoire (SODEMI). République de la Côte d'Ivoire, 180 p.

[36] Devismes, P. (1995). Atlas photographiques des minéraux des alluvions. Mémoire du BRGM, N°95, Paris, 207 p.

[37] Pojar, I., Zaharia, L., Benea, M. (2014). Heavy mineral distributions in Upper Cretaceous Bozes Formation (Apuseni Mts., Romania). Implications for sediment provenance. *Capathian. Journal of Earth and Environmental Sciences*, 9: 125 -132.

[38] Charles, N., Callec, Y., Preat, A., Thiéblemont, D., Delpondor, F., Malounguila-Nganga, D.M., Gloaguen, E., Petitot, J., Akouala, J., Ndiele, B., MvoulaBoungou, I., MoeboBoungou, M. (2015). Notice explicative de la carte géologique de la République du Congo au 1/20 000. Feuille Madingou. Edition BRGM, 221p.